PHILOSOPHICAL TRANSACTIONS OF THE ROYAL SOCIETY A MATHEMATICAL, PHYSICAL & ENGINEERING SCIENCES

# On the nucleation of cavities in planar elasticity

A. J. Levy

*Phil. Trans. R. Soc. Lond. A* 1997 **355**, 2417-2458
doi: 10.1098/rsta.1997.0142

# On the nucleation of cavities in planar elasticity

By A. J. Levy

*Department of Mechanical, Aerospace and Manufacturing Engineering, Syracuse University, Syracuse, NY 13244, USA*

## Contents



Cavity formation at an inhomogeneity is examined by analysing the problem of a plane circular elastic inclusion embedded in an unbounded elastic matrix subject to remote equibiaxial, tensile or pure shear loading. Within the framework of infinitesimal strain kinematics, nonlinear behaviour is confined to an interfacial cohesive zone characterized by a nonlinear interface force–interface separation law requiring a characteristic length for its prescription. Equilibrium solutions for symmetric and non-symmetric cavity shapes (and their associated interfacial tractions) are sought by approximation of the governing interfacial integral equations derived from the Boussinesq–Flamant solution to the problem of a point force operative at a point of a boundary. For an interval of values of characteristic length-inclusion radius ratio only a symmetric cavity will form under increasing remote load. For other parameter intervals the existence of a non-symmetric cavity is studied by performing a local bifurcation analysis about the symmetrical equilibrium state. A global, post bifurcation analysis is carried out by analysing the approximate equations computationally. Stability of equilibrium states is assessed according to the Hadamard stability definition. The complexity of cavity nucleation phenomena is revealed through the prediction of a diversity of behaviour ranging from the gradual formation of a symmetrical cavity to the gradual or abrupt formation of a non-symmetrical cavity coincident with the rigid displacement of the inclusion within the cavity. A brief, critical exam-

*Phil. Trans. R. Soc. Lond.* A (1997) **355**, 2417–2458
*Printed in Great Britain*

ination of the classical nucleation criteria (critical interfacial stress, critical energy release) is undertaken as well in light of the results of the analysis.

## 1. Introduction

In this paper we investigate the mechanics of cavity nucleation† in solid material under stress adopting the point of view that the phenomenon arises from the interaction between matrix, inclusion and the interface separating them. Furthermore, because we wish to study the formation of cavities in its barest essence, we adopt an infinitesimal strain framework and assume that nonlinear constitutive characterization is confined to a vanishingly thin interfacial cohesive zone separating an unbounded elastic matrix from a plane circular elastic inclusion. (The idea of direct constitutive modelling of the interface appears to have first been suggested by Griffith (1920) in the context of crack extension. More recently, it has been employed by Needleman (1987) in his seminal work on cavity nucleation.) The loading considered in this paper is taken to be equibiaxial, tensile, or pure shear and is assumed to be applied remotely, consistent with two dimensional states of stress and strain. Within this framework equilibrium solutions (for both symmetric and non-symmetric cavity shapes) are sought based on an integral equation formulation together with known elasticity solutions for circular domains. Brittle decohesion is treated as a problem of bifurcation of equilibrium separation at the inclusion–matrix interface under which stable non-symmetric cavities can form abruptly under uniform interface constitutive characterization and symmetric conditions of inclusion geometry and remote loading.

It is not difficult to demonstrate that the classical nucleation criteria (critical interfacial stress criterion, energy criterion) often yield incorrect or incomplete predictions of nucleation phenomena. Consider the problem of a remotely stressed unbounded matrix with elastic moduli $E$, $\nu$ containing a rigid circular inclusion of radius $R$ (figure 1). Assume that the interface is such that tangential slip can occur freely while separations normal to the interface are accompanied by relatively large interface forces. The simplest problem of nucleation occurs when the loading is a remote equibiaxial tension. In this situation cavity formation may be assumed to initiate equally from all points along the interface. Classical approaches to the prediction of cavity nucleation in such systems are based on the idea that nucleation is a critical event visited upon the inclusion rigidly bonded (in this example, against normal separation only) at all points of contact to a deformed matrix (Tanaka *et al.* 1970; Argon *et al.* 1975; Fisher & Gurland 1981). The two basic approaches (which have direct parallels in crack extension problems) are the critical interfacial stress criterion and the energy criterion alluded to previously. Thus, by the critical interfacial stress criterion, nucleation is said to occur when the uniform normal traction on the interface attains a critical value given by the interface strength $\sigma_{\max}$. For the simple system under consideration the critical remote equibiaxial stress $S_{\mathrm{S}}^{*}$ required for nucleation is given by

$$S_{\mathrm{S}}^{*} = \frac{\sigma_{\max}}{2(1-\nu)}, \tag{1.1}$$

which follows from elementary plane rotationally symmetric elastic states. Note that

† That is, the formation of an unstressed cavity from a bonded inclusion.

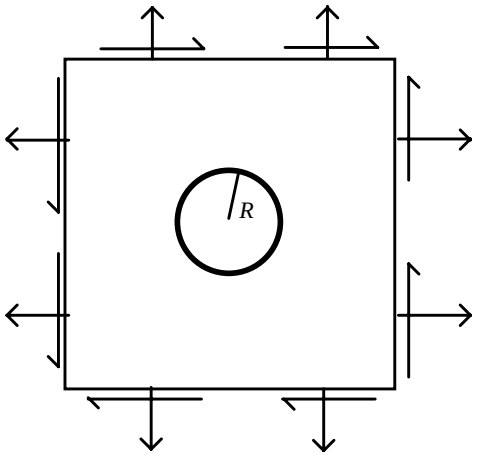


Figure 1. The planar inclusion problem.

(1.1) gives no clue as to the cavity shape after nucleation and, because only one characteristic length has been introduced in the problem, does not indicate the dependence of the critical load on inclusion radius. Furthermore, it is unclear as to precisely what event occurs when the critical load is attained since it can be expected that some separation of the (loaded) interface will in fact occur prior to the satisfaction of (1.1). (This is more readily true for weak interfaces.) The energy criterion for nucleation is an extension of the Griffith (1920) critical condition for crack growth, the difference being that the Griffith criterion for cracks is local (applying to an infinitesimal region ahead of the crack tip) while the energy criterion for nucleation can be global, applying to the entire interface. Thus, when the total potential energy stored in the rigidly bonded system becomes comparable to the total potential energy (including the work of separation per unit area of the interface, $\phi_{\rm sep}$) of the system in the fully decohered state, nucleation is said to occur. For the simple rotationally symmetric system the critical remote stress is then given by

$$S_{\rm E}^{*} = \left( \frac{1+\nu)E}{2(1-\nu)^2} \frac{\phi_{\rm sep}}{R} \right)^{1/2}, \tag{1.2}$$

where again use has been made of elementary rotationally symmetric elastic fields. Note that in (1.2) the functional dependence of the critical stress on inclusion radius occurs and is consistent with experimental observations that large inclusions nucleate cavities prior to smaller ones (Argon & Im 1975; Goods & Brown 1979; Fisher & Gurland 1981). In contrast to the critical interfacial stress criterion which fails to assert precisely what event occurs when it is satisfied, the energy criterion asserts the energetic feasibility of the transition between two well defined states. The difficulty with (1.2) is that for its derivation the 'nucleated' or fully decohered state needs to be asserted *a priori*. Obviously, this is all but impossible to do in systems subject to complex remote loading. Less obvious is the fact that even for the simplest system of rotationally symmetric geometry and loading the assumption of a rotationally symmetric nucleated state is incorrect.

In Levy (1995) is was demonstrated, by direct modelling of the interface, that for the simple system just described stable rotationally symmetric cavities must yield to the formation of stable non-symmetric cavities when the interface force attains its maximum value ($\sigma_{\rm max}$). Thus, the nucleated state is one for which the inclusion

is rigidly displaced within the cavity and so is decohered on one side of its interface and bonded, or partially bonded, on the other side. It appears then that, at least for the simple system of rotationally symmetric geometry and loading, the critical interfacial stress criterion implicitly defines nucleation to be the critical event which coincides with the possibly abrupt transition from a stable rotationally symmetric cavity to a much larger stable but non-symmetric cavity. Note, however, that prior to the attainment of the interfacial strength there is separation at the interface (which must occur for any (positive) remote stress regardless of its magnitude), while after the attainment of the interfacial strength there is still traction which acts across the interface. For this reason the critical stress criterion may give rise to critical remote loads which underestimate those required for cavity nucleation (see § 5). The energy criterion for the prediction of nucleation appears to be even less useful owing to the difficulty in defining *a priori* the nucleated state needed to implement the criterion.

When the (planar) remote loading is anything other then equibiaxial, the definition and prediction of nucleation by the classical criteria becomes even more ambiguous. To see this let the remote load be a tensile stress acting on the system just considered. The critical interfacial stress criterion yields

$$S_{\mathrm{S}}^{*} = \frac{5 - 6\nu}{(11 - 6\nu)(1 - \nu)}\sigma_{\max}, \tag{1.3}$$

where use has been made of the fact that the maximum interfacial traction occurs at the two points where the radii are in line with the remote load. In deriving (1.3), it is understood that the matrix elastic fields are obtained from interface boundary conditions of normal displacement continuity and vanishing shear traction (Muskhelishvili 1953). Because separation will occur (when the interface is modeled directly) prior to the attainment of (1.3), and because it will generally not be true that (1.3) is associated with some abrupt change in cavity shape, it is unclear as to precisely what critical event is predicted with the satisfaction of (1.3). If the energy criterion is employed, the total potential energy prior to nucleation may be calculated from the elastic fields used to obtain (1.3), however, as for the case of remote equibiaxial loading, it is not obvious how to choose the state after nucleation. In Tanaka *et al.* (1970) the nucleated state is chosen to be such that the interface is free of stress in the two regions of interface whose normals are approximately in line with the direction of loading, while everywhere else the matrix is in mechanical contact with the inclusion. This assumption presupposes that the inclusion does not displace rigidly at some point in the nucleation process (a hypothesis which may not be valid given that in our example the interface does not support shear traction). One purpose of the present work is to rigorously analyse the onset of nucleation in a simple system and to assess nucleation criteria within that framework.

The paper is organized as follows. In § 2, the formulation of the governing integral equations is reviewed and a reduction to a truncated set of nonlinear algebraic equations is carried out. Necessary conditions for bifurcation of equilibrium cavity shapes are presented as well. Section 3 contains detailed local analyses of bifurcation behaviour under increasing remote equibiaxial load (two mode approximation), tensile load (three mode approximation) and shear load (three mode approximation). A global bifurcation analysis is carried out in § 4 by numerically solving the governing equations. Higher-order approximations are obtained for post bifurcation behaviour and, in order to confirm the predictions, of the lower-order local analyses of § 3. The paper concludes with a brief critical assessment of the classical nucleation criteria and closing comments.

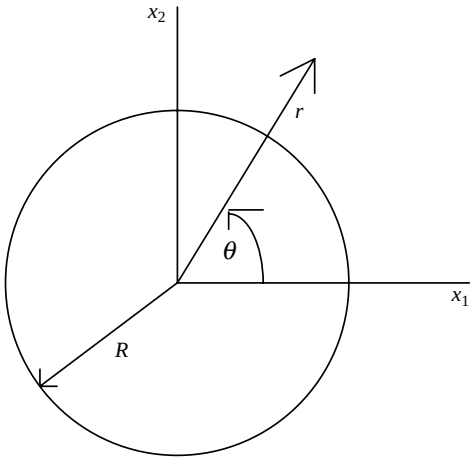


Figure 2. The circular inclusion.

## 2. Basic formulation

Consider a plane circular region $\mathcal{R}$ (the inclusion), bounded by a closed curve $\partial\mathcal{R}$ with unit normal $\boldsymbol{n}$ and elastic moduli $E^*$, $\nu^*$ contained within an unbounded matrix with elastic moduli $E$, $\nu$. Fix a Cartesian system† with origin at the inclusion centre, point coordinates $(x_1, x_2)$, base vectors $(\boldsymbol{e}_1, \boldsymbol{e}_2)$ and introduce a polar coordinate system with coordinates $(r, \theta)$ and base vectors $(\boldsymbol{e}_r, \boldsymbol{e}_\theta)$ (figure 2). Assume that the remote loading is a planar stress given by $\boldsymbol{S}^\infty = S_{11}^\infty \boldsymbol{e}_1 \otimes \boldsymbol{e}_1 + S_{22}^\infty \boldsymbol{e}_2 \otimes \boldsymbol{e}_2 + \nu(S_{11}^\infty + S_{22}^\infty)\boldsymbol{e}_3 \otimes \boldsymbol{e}_2$ applied at $r \to \infty$. By the spectral decomposition theorem this form is the most general planar remote loading so that $S_{11}^\infty = S_{22}^\infty$ indicates equibiaxial loading, $S_{22}^\infty = 0$ indicates tensile loading, $S_{11}^\infty = -S_{22}^\infty$ indicates pure shear loading, etc. Further assume that the interface cannot support shear and is such that a uniform nonlinear constitutive relation couples the normal component of interface traction $(f)$ to the normal component of displacement jump $([u_r])$ across the interface. Then the interface traction vector $\boldsymbol{s}_\mathrm{I}$ may be expressed in the form

$$\boldsymbol{s}_\mathrm{I}(\boldsymbol{n}; [u_r]) = f([u_r])\boldsymbol{n}, \tag{2.1}$$

where the explicit functional dependence of $f$ on the interface coordinate $(\theta)$ is absent owing to the assumed uniformity of the interface. Now owing to the rotational symmetry of the geometry and the uniformity of the interface force law, cavities symmetric with respect to the $\boldsymbol{e}_1$–$\boldsymbol{e}_3$ and $\boldsymbol{e}_2$–$\boldsymbol{e}_3$ planes can be expected to form under the action of the remote load $\boldsymbol{S}^\infty$. Stable non-symmetric cavities can be expected to form as well, provided that the physical and geometrical parameters of the problem assume certain values. A general framework for the prediction of symmetric and non-symmetric cavity formation in systems subject to complex remote load and an interface force (2.1) has been presented by Levy (1991) in the form of integral equations governing the separation at a circular interface. Certain of those results are presented below without derivation.

For arbitrary, planar remote loads, the (Fredholm) integral equation governing the normalized radial component of displacement jump $(u = [u_r]/R)$ has been shown to

† Tensor notation used in this paper is consistent with Gurtin (1984).

be of the form

$$u(\theta) = h_r(\theta) + \int_0^{2\pi} f(u(\theta'))K_r(\theta - \theta')\,\mathrm{d}\theta', \tag{2.2}$$

where $K_r$ is a symmetric, weakly singular kernel. The term $h_r$ is the (normalized) radial displacement of the inner boundary of a circular cavity in remote stress field $\boldsymbol{S}^\infty$ and is proportional to linear combinations of the ratios $S^\infty_{11}/E$, $S^\infty_{22}/E$. The normalized circumferential component $v = [u_\theta]/R$ has been shown to be governed by an integral expression

$$v(\theta) = h_\theta(\theta) + \int_0^{2\pi} f(u(\theta'))K_\theta(\theta - \theta')\,\mathrm{d}\theta', \tag{2.3}$$

where $h_\theta$ is the normalized circumferential displacement at the inner boundary of a circular cavity (also proportional to linear combinations of the ratios $S^\infty_{11}/E$, $S^\infty_{22}/E$). Note that in (2.3), $v$ is determined by integration once the integral equation (2.2) has been solved for $u$. In order to complete the description, rigid-body force equilibrium of the inclusion is enforced through the integral equations

$$\int_0^{2\pi} f(u(\theta'))\cos(\theta')\,\mathrm{d}\theta' = 0, \quad \int_0^{2\pi} f(u(\theta'))\sin(\theta')\,\mathrm{d}\theta' = 0. \tag{2.4}$$

Moment equilibrium is guaranteed through the interface force law assumption (2.1). Explicit expressions for $K_r$, $K_\theta$ and $h_r$, $h_\theta$ are given in Appendix A.

Nonlinear integral equations of the type given by (2.2) can be put in the standard Hammerstein form

$$u(\theta) + \int_0^{2\pi} F(\theta', u(\theta'))\tilde{K}(\theta, \theta')\,\mathrm{d}\theta' = 0, \tag{2.5}$$

by writing $h_r$ (given explicitly by (A 6)) in the form $h_r(\theta) = \int_0^{2\pi} g(\theta)K_r(\theta - \theta')\,\mathrm{d}\theta'$. This linear Fredholm integral equation of the first kind can be easily solved for $g$ (note (A 1)–(A 4)), so that $F$ in (2.5) has the representation $F = f(u) + \lambda_0 h_0 + \lambda_3 h_3 \cos 2\theta$, where $\lambda_0$, $\lambda_3$ are eigenvalues of the kernel $K_r$ given by (A 2), (A 3) and $h_0$, $h_3$ are given in (A 6). Note that in (2.5), $\tilde{K} = -K_r$. The basic conditions required for Hammerstein's theorem on the existence of solutions to (2.5) are that (i) the kernel be symmetric, (ii) the kernel be quadratically integrable and (iii) the kernel have positive eigenvalues. These conditions are seen to hold for $\tilde{K}$ $(= -K_r)$ (Levy 1991). Furthermore, a continuous solution to (2.5) will exist, provided the function $F$ is contiuuous and such that it satisfies the condition

$$|F(u, \theta)| = |f(u) + \lambda_0 h_0 + \lambda_3 h_3 \cos 2\theta| \leqslant C_1|u| + C_2, \tag{2.6}$$

where $C_1$ and $C_2$ are positive constants and $C_1$ is less than the first eigenvalue $-\lambda_0$ of the positive kernel $\tilde{K}$. Thus, (2.6) contrains the functional form of the interface force law $f$ required to yield solutions to (2.2). Assume that $f$ is such that it satisfies (2.6).

Now the symmetry of the kernel $K_r$ and the proof of Hammerstein's theorem (Tricomi 1985) on the existence of solutions to (2.5) suggest that an approximate solution to (2.2) (and (2.4)) be sought in the form of an eigenfunction expansion,

$$u(\theta) = \sqrt{2\pi}u_0\varphi_0 + \sqrt{\pi}\sum_{i=1}^{n} u_i\varphi_i(\theta), \tag{2.7}$$

where the $\varphi_i$ are the orthonormal eigenfunctions given by (A 4) and the $u_i$ are the unknown coefficients determined so as to satisfy (2.2) and (2.4). The expansion (2.7), along with the orthogonality of the eigenfunctions, reduces (2.2) and (2.4) to a system of $n+1$ nonlinear algebraic equations governing the $n+1$ coefficients $u_0$, $u_i$, $i = 1, 2, \ldots, n$:

$$\sqrt{2\pi}u_0 - \frac{1}{\lambda_0}\int_0^{2\pi} f(u_i;\theta')\varphi_0 \,\mathrm{d}\theta' - \sqrt{2\pi}h_0 = 0, \tag{2.8 a}$$

$$\int_0^{2\pi} f(u_i;\theta')\varphi_1(\theta') \,\mathrm{d}\theta' = 0, \tag{2.8 b}$$

$$\int_0^{2\pi} f(u_i;\theta')\varphi_2(\theta') \,\mathrm{d}\theta' = 0, \tag{2.8 c}$$

$$\sqrt{\pi}u_3 - \frac{1}{\lambda_3}\int_0^{2\pi} f(u_i;\theta')\varphi_3(\theta') \,\mathrm{d}\theta' - \sqrt{\pi}h_3 = 0, \tag{2.8 d}$$

$$\sqrt{\pi}u_j - \frac{1}{\lambda_j}\int_0^{2\pi} f(u_i;\theta')\varphi_j(\theta') \,\mathrm{d}\theta' = 0, \quad j = 4, 5, \ldots, n. \tag{2.8 e}$$

Without loss of generality assume that the remote loading $\boldsymbol{S}^\infty$ is such that $S_{11}^\infty > 0$ so that even solutions exist, i.e. $u_{2p} = 0$, $p = 1, 2, \ldots$ (This follows from the fact that $f(u_1;\theta)$ will be even in $\theta$ and (2.8 *c*) and (2.8 *e*) (with $j = 2p$, $p = 2, 3, \ldots$) are identically satisfied owing to the vanishing of the integral, from 0 to $2\pi$, of an odd function.) Solutions to the modified system,

$$\sqrt{2\pi}u_0 - \frac{1}{\lambda_0}\int_0^{2\pi} f(u_0, u_{2i-1};\theta')\varphi_0 \,\mathrm{d}\theta' - \sqrt{2\pi}h_0 = 0, \tag{2.9 a}$$

$$\int_0^{2\pi} f(u_0, u_{2i-1};\theta')\varphi_1(\theta') \,\mathrm{d}\theta' = 0, \tag{2.9 b}$$

$$\sqrt{\pi}u_3 - \frac{1}{\lambda_3}\int_0^{2\pi} f(u_0, u_{2i-1};\theta')\varphi_3(\theta') \,\mathrm{d}\theta' - \sqrt{\pi}h_3 = 0, \tag{2.9 c}$$

$$\sqrt{\pi}u_{2j-1} - \frac{1}{\lambda_{2j-1}}\int_0^{2\pi} f(u_0, u_{2i-1};\theta')\varphi_{2j-1}(\theta') \,\mathrm{d}\theta' = 0, \quad j = 3, 4, \ldots, \tag{2.9 d}$$

may now be taken in the form

$$u(\theta) = \sqrt{2\pi}u_0\varphi_0 + \sqrt{\pi}\sum_{i=1}^{n} u_{2i-1}\varphi_{2i-1}(\theta), \tag{2.10}$$

with $\varphi_0 = 1/\sqrt{2\pi}$, $\varphi_{2i-1} = \cos i\theta/\sqrt{\pi}$. We expect that there will be symmetrical solutions (with respect to the $\boldsymbol{e}_2 - \boldsymbol{e}_3$ plane) to (2.10) for some range of physical and geometrical parameters. (The proof of this assertion, i.e. that $u_{2k-1} = 0$, $k = 1, 3, 5, \ldots$, satisfies (2.9 *b*), (2.9 *d*) with $j$ odd, is given in Appendix B.) Symmetrical solutions $u(\theta) = u(\theta + \pi)$ (with zero rigid-body displacement) are of the form $u = u_0 + \sum_{p=1}^{n} u_{4p-1}\cos 2p\theta$, with the remaining coefficients governed by (2.9 *a*), (2.9 *c*), (2.9 *d*) with $j$ even. In the following sequel we assume all parameters which arise in the description of the interface force law to be fixed along with the inclusion radius ($R$) and the material properties of matrix and inclusion. We seek the behaviour

of solutions to (2.9) under a varying measure of remote loading characterized by $h_0$, $h_3$ (A 6). In particular, we are concerned with bifurcations from symmetrical equilibrium cavity shapes (which are assumed to occur for small measures of remote loading) to either adjacent symmetrical cavity shapes, or to non-symmetrical cavity shapes. The implicit function theorem implies that equilibria described by smooth functions of bifurcation parameter exist at those values for which the Jacobian determinant of the nonlinear algebraic system is non-vanishing. Thus, a necessary condition for bifurcation, i.e. for different branches of equilibria to meet, is for the determinant of the Jacobian matrix $\boldsymbol{J}$ to vanish. For the system (2.9), we have $\det \boldsymbol{J} = 0$, where $\det \boldsymbol{J}$ is given by

$$\begin{vmatrix} \mathrm{A} & 0 & \mathrm{B} & 0 & \cdots \\ 0 & \mathrm{C} & 0 & \mathrm{D} & \cdots \\ \mathrm{E} & 0 & \mathrm{F} & 0 & \cdots \\ 0 & \mathrm{G} & 0 & \mathrm{H} & \cdots \\ \vdots & \vdots & \vdots & \vdots & \end{vmatrix}. \tag{2.11}$$

where

$$\mathrm{A} = 1 - \frac{\lambda_0^{-1}}{2\pi}\int_0^{2\pi} D_u f \,\mathrm{d}\theta, \quad \mathrm{B} = -\frac{\lambda_0^{-1}}{2\pi}\int_0^{2\pi} D_u f \cos 2\theta \,\mathrm{d}\theta,$$

$$\mathrm{C} = \frac{1}{\sqrt{\pi}}\int_0^{2\pi} D_u f \cos^2\theta \,\mathrm{d}\theta, \quad \mathrm{D} = \frac{1}{\sqrt{\pi}}\int_0^{2\pi} D_u f \cos\theta \cos 3\theta \,\mathrm{d}\theta,$$

$$\mathrm{E} = -\frac{\lambda_3^{-1}}{\pi}\int_0^{2\pi} D_u f \cos 2\theta \,\mathrm{d}\theta, \quad \mathrm{F} = 1 - \frac{\lambda_3^{-1}}{\pi}\int_0^{2\pi} D_u f \cos^2 2\theta \,\mathrm{d}\theta,$$

$$\mathrm{G} = -\frac{\lambda_5^{-1}}{\pi}\int_0^{2\pi} D_u f \cos 3\theta \cos\theta \,\mathrm{d}\theta, \quad \mathrm{H} = 1 - \frac{\lambda_5^{-1}}{\pi}\int_0^{2\pi} D_u f \cos^2 3\theta \,\mathrm{d}\theta.$$

Note that $\det \boldsymbol{J}$ is evaluated at the symmetrical solution so that $D_u f(\theta) = D_u f(\theta + \pi)$. In the expression for $\det \boldsymbol{J}$, use has been made of the fact that integrals of the form

$$I_{ij} = \int_0^{2\pi} \Gamma(\theta) \cos i\theta \cos j\theta \,\mathrm{d}\theta,$$

with $\Gamma(\theta) = \Gamma(\theta + \pi)$, are such that

$$I_{ij} = \begin{cases} 0, & i \text{ odd}, \quad j \text{ even}, \\ 2\displaystyle\int_0^{\pi} \Gamma(\theta) \cos i\theta \cos j\theta \,\mathrm{d}\theta, & i, j \text{ odd}, \\ 2\displaystyle\int_0^{\pi} \Gamma(\theta) \cos i\theta \cos j\theta \,\mathrm{d}\theta, & i, j \text{ even}. \end{cases}$$

(For proof of this assertion see Appendix B.) Owing to the alternating null entries in the Jacobian determinant it is possible to write $\det \boldsymbol{J}$ as the product of two lower-

order determinants $\det \boldsymbol{J}_s$, $\det \boldsymbol{J}_u$ given by

$$\det \boldsymbol{J}_s = \begin{vmatrix} 1 - \dfrac{\lambda_0^{-1}}{2\pi}\displaystyle\int_0^{2\pi} D_u f \,\mathrm{d}\theta & -\dfrac{\lambda_0^{-1}}{2\pi}\displaystyle\int_0^{2\pi} D_u f \cos 2\theta \,\mathrm{d}\theta & \cdots \\ -\dfrac{\lambda_3^{-1}}{\pi}\displaystyle\int_0^{2\pi} D_u f \cos 2\theta \,\mathrm{d}\theta & 1 - \dfrac{\lambda_3^{-1}}{\pi}\displaystyle\int_0^{2\pi} D_u f \cos^2 2\theta \,\mathrm{d}\theta & \cdots \\ \vdots & \vdots & \end{vmatrix}, \tag{2.13}$$

$$\det \boldsymbol{J}_u = \begin{vmatrix} \dfrac{1}{\sqrt{\pi}}\displaystyle\int_0^{2\pi} D_u f \cos^2\theta \,\mathrm{d}\theta & \dfrac{1}{\sqrt{\pi}}\displaystyle\int_0^{2\pi} D_u f \cos\theta \cos 3\theta \,\mathrm{d}\theta & \cdots \\ -\dfrac{\lambda_5^{-1}}{\pi}\displaystyle\int_0^{2\pi} D_u f \cos 3\theta \cos\theta \,\mathrm{d}\theta & 1 - \dfrac{\lambda_5^{-1}}{\pi}\displaystyle\int_0^{2\pi} D_u f \cos^2 3\theta \,\mathrm{d}\theta & \cdots \\ \vdots & \vdots & \end{vmatrix}. \tag{2.14}$$

Thus, the vanishing of either $\det \boldsymbol{J}_s$ or $\det \boldsymbol{J}_u$ is a necessary condition for bifurcation of the symmetrical solution $u$. Furthermore, the condition $\det \boldsymbol{J}_s = 0$ governs symmetrical bifurcations, i.e. transitions from a symmetrical equilibrium state to a symmetrical equilibrium state, while $\det \boldsymbol{J}_u = 0$ governs non-symmetrical bifurcations (transitions from a symmetrical equilibrium state to a non-symmetrical equilibrium state). This follows from the fact that (2.9 *b*) and (2.9 *d*) with $j$ odd are identically satisfied for symmetrical solutions.

Both $\det \boldsymbol{J}_s = 0$ and $\det \boldsymbol{J}_u = 0$ represent constraints on the slope of the interface force–separation curve required for bifurcation. For the case where the remote load is equibiaxial ($S_{11}^{\infty} = S_{22}^{\infty}$), the constraint $\det \boldsymbol{J}_u = 0$ takes on a particularly simple form. To see this note that (A 6) implies that $h_3 = 0$ and so rotationally symmetric solutions to (2.9) are uniform and given by $\hat{u}, u_i = 0$, $i = 1, 2, \ldots$. In this situation the system (2.9) reduces to a single nonlinear algebraic equation governing $\hat{u}_0$:

$$\hat{u}_0 - \lambda_0^{-1} f(\hat{u}_0) - h_0 = 0. \tag{2.15}$$

Noting that $D_{u_0} f$ is now uniform, independent of $\theta$, the symmetric and non-symmetric bifurcation conditions assume the form

$$\det \boldsymbol{J}_s = \begin{vmatrix} 1 - \lambda_0^{-1} D_{u_0} f & 0 & 0 & \cdots \\ 0 & 1 - \lambda_3^{-1} D_{u_0} f & 0 & \cdots \\ \vdots & \vdots & \vdots & \end{vmatrix},$$

$$\det \boldsymbol{J}_u = \begin{vmatrix} D_{u_0} & 0 & 0 & \cdots \\ 0 & 1 - \lambda_5^{-1} D_{u_0} f & 0 & \cdots \\ \vdots & \vdots & \vdots & \end{vmatrix}.$$

Now assume that the interface force is such that it is monotonically increasing on $(-\infty, u_{\max})$, monotonically decreasing on $(u_{\max}, \infty)$ and such that $u_{\max} > 0$ and $f(0) = 0$. Then, because the eigenvalues $\lambda_i$ are all negative, an inspection of the bifurcation conditions reveal that a non-symmetric bifurcation occurs (when $D_{u_0} f = 0$) prior to a symmetric one which must occur when the interface force is on the descending branch of the interface force–separation curve. Thus, bifurcation under remote

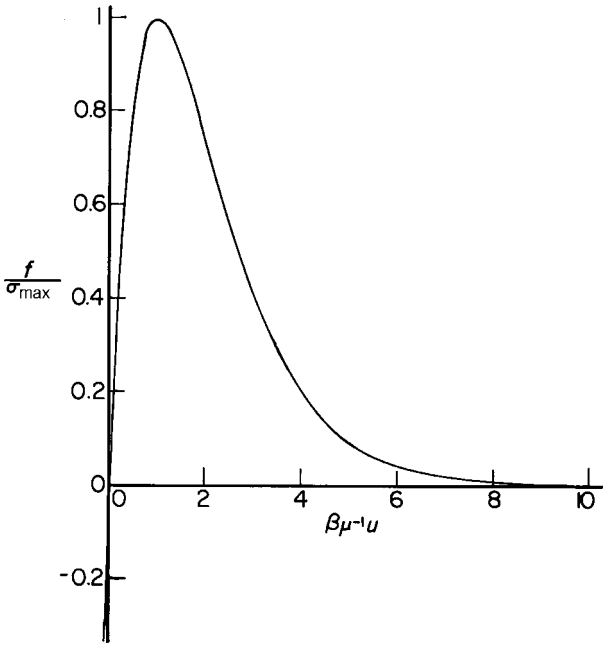


Figure 3. The interface force law.

equibiaxial loading first occurs when the interface force law attains its maximum value. (Symmetric and non-symmetric bifurcations of (2.15) have been studied in detail in Levy (1994) and Levy (1995), respectively.) Unfortunately, when the remote loading is other then equibiaxial a simple bifurcation condition (analogous to $D_{u_0} f = 0$) no longer exists, in part because $D_u f$ is no longer uniform. If $D_u f$ is expanded in a Fourier series in eigenfunctions $1/\sqrt{2\pi}$, $\cos 2p\theta/\sqrt{\pi}$, then the vanishing of (2.13) and (2.14) each represent an equation relating the coefficients in the expansion. These relations, which characterize how the interfacial traction is distributed at bifurcation, are extremely complicated and contain little physical or geometrical insight in their general form. They will not be presented here although distributions of interfacial traction at bifurcation will be presented in § 4 for a specific functional form of $f$.

The (normalized) circumferential displacement jump $v$ ($= [u_\theta]/R$) is fixed, through (2.3), by the normal component of normalized displacement jump $u$ (recall that the inclusion is assumed to be smooth so that no tangential tractions develop at the interface). Thus, $v$ follows from an expansion of the type (2.7), i.e.

$$v(\theta) = \sqrt{2\pi} v_0 \varphi_0 + \sqrt{\pi} \sum_{i=1}^{n} v_i \varphi_i(\theta), \tag{2.16}$$

where the eigenfunctions $\varphi_i$ are given in Appendix A. In order to determine the expanded form of the integral expression (2.3), substitute (2.16) into (2.3) making use of expansions for $u$ (2.7), for $K_\theta$ (A 5), and for $h_\theta$ (A 6). Orthogonality of eigenfunctions yields the mode multipliers $v_i$:

$$v_0 = 0,$$

$$v_{2n} = \frac{1}{\sqrt{\pi}} \int_0^{2\pi} h_\theta(\theta) \varphi_{2n}(\theta)\, \mathrm{d}\theta + \frac{c + c'n}{\sqrt{\pi}(n^2 - 1)} \int_0^{2\pi} f(u_k; \theta) \varphi_{2n-1}(\theta)\, \mathrm{d}\theta,$$

$$v_{2n-1} = \frac{1}{\sqrt{\pi}} \int_0^{2\pi} h_\theta(\theta)\varphi_{2n-1}(\theta)\,\mathrm{d}\theta - \frac{c + c'n}{\sqrt{\pi}(n^2-1)} \int_0^{2\pi} f(u_k;\theta)\varphi_{2n}(\theta)\,\mathrm{d}\theta, \qquad n = 2, 3, \ldots,$$

where $c$, $c'$ follow from (A 5). Note that coefficients in $v$ which are proportional to $\sin\theta$ and $\cos\theta$ do not appear in the expressions for $v_i$ owing to the fact that rigid-body equilibrium conditions (2.4) constrain the coefficients $v_1$, $v_2$ to be such that $v_1 = u_2$, $v_2 = -u_1$. If the inclusion is taken to be rigid, and non-symmetric separation is assumed to be even in $\theta$ ($u_{2n} = 0$, $n = 1, 2, 3, \ldots$), then the mode multipliers assume the form

$$v_0 = 0, \quad v_1 = 0, \quad v_2 = -u_1, \quad v_{2n-1} = 0,$$

$$v_{2n} = \frac{1}{\pi} \int_0^{2\pi} h_\theta(\theta) \sin n\theta\,\mathrm{d}\theta + \frac{1}{\pi(n^2-1)} \left[\frac{2(1-\nu^2)}{E} + n\frac{(1+\nu)(1-2\nu)}{E}\right] \times \int_0^{2\pi} f(u_k;\theta)\cos n\theta\,\mathrm{d}\theta, \quad n = 2, 3, \ldots. \tag{2.17}$$

The circumferential displacement jump $v$ then follows directly from (2.16), (2.17) and the mode multipliers $u_i$.

We assume for the remainder of the paper that the interface traction $f$ is governed by the physically based force law of Ferrante *et al.* (1982) given by

$$f : u \to e\sigma_{\max}\beta(u/\mu)\exp(-\beta u/\mu) \tag{2.18}$$

and depicted in figure 3. In (2.18), $\sigma_{\max}$ is the interface strength, $\mu$ is the (positive) length parameter, i.e. the ratio of force length† ($\delta > 0$) to inclusion radius ($R$), $\beta$ is a fit parameter which can be arbitrarily set provided $\delta$ is regarded as a phenomenological parameter and $\mathrm{e} = \exp(1)$. (The value $\beta = 4.8325$ is that for which the work of separation of (2.18) is equal to the work of separation for the third degree polynomial approximation of $f$.) Note that this force law satisfies the requirement (2.6) for the existence of solutions to governing integral equation (2.2).

## 3. The bifurcation problem

### (*a*) *General results for the three mode approximation*

In this section we analyse the character of local bifurcations in a reduced system subject to remote equibiaxial load, remote tension and remote pure shear. Although not formally demonstrated, it is tacitly assumed through most of this section that bifurcation behaviour in the reduced system carries over to the exact solution of (2.2), (2.4) and (2.18), at least qualitatively. (This assumption will be considered further in the next section where higher-order approximations to the exact solution are shown to yield qualitatively similar results for equibiaxial and tension loading but not for pure shear loading.) Now consider the radial interfacial separation $u(\theta)$ to be composed of two symmetric modes and one non-symmetric rigid-body mode,

$$u(\theta) = u_0 + u_1\cos\theta + u_3\cos 2\theta,$$

where the coefficients $u_0$, $u_1$, $u_3$ are governed by the three term approximation of (2.9). It is convenient to write the three mode system in terms of the dimensionless

† Physically, $\delta$ characterizes the range of action of the force law (2.18).

variables $w_0$, $w_1$, $w_3$, defined by

$$w_1 + \beta u_i \mu^{-1}, \quad i = 0, 1, 3, \tag{3.1}$$

and also to be such that the Jacobian matrix is symmetric. Thus, $F_i(w_0, w_1, w_3) = 0$, $i = 1, 2, 3$, where

$$\begin{aligned}
F_1(w_i) &= \mu w_0 - \beta h_0 + \frac{\alpha_0}{2\pi}\int_0^{2\pi} (w_0 + w_1\cos\theta + w_3\cos 2\theta)\mathrm{e}^{-(w_0 + w_1\cos\theta + w_3\cos 2\theta)}\,\mathrm{d}\theta,\\
F_2(w_i) &= \frac{\alpha_0}{2\pi}\int_0^{2\pi} (w_0 + w_1\cos\theta + w_3\cos 2\theta)\mathrm{e}^{-(w_0 + w_1\cos\theta + w_3\cos 2\theta)}\cos\theta\,\mathrm{d}\theta,\\
F_3(w_i) &= \frac{\alpha_0}{2\alpha_3}(\mu w_3 - \beta h_3)\\
&\quad + \frac{\alpha_0}{2\pi}\int_0^{2\pi} (w_0 + w_1\cos\theta + w_3\cos 2\theta)\mathrm{e}^{-(w_0 + w_1\cos\theta + w_3\cos 2\theta)}\cos 2\theta\,\mathrm{d}\theta
\end{aligned} \tag{3.2}$$

and $\alpha_1 = -e\sigma_{\max}\lambda_1^{-1}\beta > 0$ (recall the eigenvalues $\lambda_i$ are negative (A 3)). The symmetrical solution $(\hat{w}_0, 0, \hat{w}_3)$ satisfies the system $F(w_0, w_1, w_3) = 0$, provided $\hat{w}_0$, $\hat{w}_3$ are solutions to the nonlinear equations

$$F_1(\hat{w}_0, 0, \hat{w}_3) = \mu\hat{w}_0 - \beta h_0 + \alpha_0\mathrm{e}^{-\hat{w}_0}[\hat{w}_0 I_0(\hat{w}_3) - \hat{w}_3 I_1(\hat{w}_3)] = 0, \tag{3.3a}$$

$$F_3(\hat{w}_0, 0, \hat{w}_3) = \frac{\alpha_0}{2\alpha_3}(\mu\hat{w}_3 - \beta h_3) + \alpha_0\mathrm{e}^{-\hat{w}_0}[-(1 + \hat{w}_0)I_1(\hat{w}_3) + \hat{w}_3 I_0(\hat{w}_3)] = 0, \tag{3.3b}$$

where $I_n$ is the modified Bessel function of the first kind of order $n$. (For this solution, $F_2(\hat{w}_0, 0, \hat{w}_3) = 0$ is satisfied identically.) Note that, in deriving (3.3), use has been made of the result (Gradshteyn & Ryzhik 1994)

$$\int_0^{2\pi} \cos mz \exp(p\cos z)\,\mathrm{d}z = 2\pi I_m(p) \tag{3.4}$$

and the recursion formulas connecting the $I_n$ (Watson 1995). The Jacobian determinants $\det \boldsymbol{J}_s$ (2.13) and $\det \boldsymbol{J}_u$ (2.14) for the three mode approximation and the notation (3.1) may be written in the symmetrical forms

$$\det \boldsymbol{J}_s = \begin{vmatrix} \mathrm{A} & \mathrm{B} \\ \mathrm{B} & \mathrm{C} \end{vmatrix}, \tag{3.5a}$$

where

$$\begin{aligned}
\mathrm{A} &= \mu + \alpha_0\mathrm{e}^{-w_0}[(1 - w_0)I_0 + w_3 I_1],\\
\mathrm{B} &= \alpha_0\mathrm{e}^{-w_0}[w_0 I_1 - w_3 I_0],\\
\mathrm{C} &= \frac{\mu\alpha_0}{2\alpha_3} + \alpha_0\mathrm{e}^{-w_0}[(w_3 + w_3^{-1} + w_0 w_3^{-1})I_1 - w_0 I_0],
\end{aligned}$$

and

$$\det \boldsymbol{J}_u = \tfrac{1}{2}\alpha_0\mathrm{e}^{-w_0}[(1 - w_0 - w_3)I_0 + (w_0 + w_3)I_1], \tag{3.5b}$$

where it is understood that the argument of the Bessel functions is $w_3$. For a given remote loading $(h_0, h_3)$, (3.1) and (3.3) can be solved for the coefficients $(u_0, u_3)$, yielding the two mode symmetrical solution $u(\theta) = u_0 + u_3\cos 2\theta$. Calculations for

the solution under various remote loads are postponed until the next section when higher-order approximations will be computed numerically. Here we are concerned primarily with the character of bifurcations which occur from symmetrical solution states and so we seek those (bifurcation) points corresponding to solutions of (3.3) subject to either of the constraints $\det \boldsymbol{J}_s = 0$, $\det \boldsymbol{J}_u = 0$.

At this stage there is no reason to assert that the stability† of the equilibrium states before and after bifurcation can be assessed within the usual framework of finite dimensional dynamical systems theory, i.e. according to the signs of the eigenvalues of the Jacobian matrix of the vector field‡ evaluated at the equilibrium point. In the present development we are concerned with equilibrium states governed by equations which have been derived from elastostatics, so that information on the stability of a particular equilibrium state can only be obtained with the introduction of an additional criterion. In the present work we adopt Hadamard's definition of stability (herein called Hadamard stability) based on the statical energy criterion (Knops & Wilkes 1973). Thus, for our approximate non-dissipative inclusion–interface matrix system we assert the existence of a total potential energy function which depends on the three separation modes, i.e. $\Phi : \{u_0, u_1, u_3\} \to \Phi(u_0, u_1, u_3)$, and which can be defined through its gradients according to

$$\frac{\partial \Phi}{\partial u_0} = \beta\mu^{-1} F_1, \tag{3.6 a}$$

$$\frac{\partial \Phi}{\partial u_1} = \beta\mu^{-1} F_2, \tag{3.6 b}$$

$$\frac{\partial \Phi}{\partial u_3} = \beta\mu^{-1} F_3, \tag{3.6 c}$$

where the $F_i$ are given in (3.2) and use has been made of (3.1). Hadamard's stability criterion defines an equilibrium state $\{\hat{u}_0, \hat{u}_1, \hat{u}_3\}$ to be locally stable provided that the total potential energy $\Phi$ evaluated at a point $\{u_0, u_1, u_3\}$, contained in a neighbourhood of $\{\hat{u}_0, \hat{u}_1, \hat{u}_3\}$, is such that $\Phi(u_0, u_1, u_3) > \Phi(\hat{u}_0, \hat{u}_1, \hat{u}_3)$. This criterion may be expressed in terms of the positive definiteness of the quadratic form, $Q(\xi_0, \xi_1, \xi_3) = \sum_{i,j=0,1,3} \partial^2 \Phi/(\partial u_i \partial u_j)\xi_i \xi_j$, evaluated at the equilibrium state being tested. A sufficient condition for local stability is therefore that the eigenvalues $(\omega_0, \omega_1, \omega_3)$ of $Q(\xi_0, \xi_1, \xi_3) = \omega_0\xi_0^2 + \omega_1\xi_1^2 + \omega_3\xi_3^2$ be positive at the equilibrium being tested. By virtue of (3.6), we can now assert that Hadamard stability of equilibria is equivalent to requiring positive eigenvalues of the Jacobian matrix of partial derivatives of the $F_i$ ((3.2)) (evaluated at equilibrium).

In the following subsections, local bifurcation analyses are carried out for the case of remote equibiaxial load, remote tensile load and remote pure shear load.

### (*b*) *Equibiaxial load*

For the case where the remote load is equibiaxial, $S_{11}^{\infty} = S_{22}^{\infty}$ and $h_3 = 0$, so that the bifurcation parameter $h_0$ is given by $h_0 = 2(1 - \nu^2)S_{11}^{\infty}/E$. Then (3.3) and (3.5) reduce to

$$F_1(w_0) = \mu w_0 + \alpha_0 \mathrm{e}^{-w_0} w_0 - \beta h_0 = 0, \tag{3.7 a}$$

$$\det \boldsymbol{J}_u = 1 - w_0 = 0, \tag{3.7 b}$$

† Stability in the sense of Liapounov (Hirsch & Smale 1974).

‡ That is, vector field $F : R^n \to R^n$ in $x' + F(x) = 0$.

$$\det \boldsymbol{J}_s = \mu + \alpha_0 \mathrm{e}^{-w_0}(1 - w_0) = 0. \tag{3.7\,c}$$

Clearly, bifurcation will first occur when $\det \boldsymbol{J}_u$ vanishes, since $\det \boldsymbol{J}_s$ is positive for $w_0 \in [0, 1]$. Thus, non-symmetrical bifurcation will occur when $w_0 = 1$ which, with the help of (3.6 *a*), may be written as

$$\mu + \beta\left[(1+\nu^*)(1-2\nu)\frac{\sigma_{\max}}{E} + (1+\nu)\frac{\sigma_{\max}}{E}\right] - 2(1-\nu^2)\beta\frac{S_{11}^{\infty}}{E} = 0, \tag{3.8}$$

where use has been made of (A 2) (recall that $\alpha_1 = -e\sigma_{\max}\lambda_1^{-1}\beta$). This equation may be used to find the critical value of remote load required to precipitate non-symmetrical decohesion. Note that $w_0 = 1$ corresponds to $u_0 = \mu\beta^{-1}$ which, from (2.18), locates the maximum interface traction attainable $\sigma_{\max}$. Thus, transition occurs when the interface force reaches its maximum value. Furthermore, because the pre-bifurcated state under equibiaxial loading is rotationally symmetric (and therefore describable by a single uniform mode), the results obtained are exact and consistent with Levy (1994, 1995).

From herein we assume the following values for the constitutive properties of the matrix, inclusion and interface:

$$\sigma_{\max} = 0.006E, \quad \nu = 0.30, \quad E^* \to \infty \text{ (rigid inclusion)}, \quad \beta = 4.8325, \tag{3.9}$$

which fix $\beta$, $\alpha_0$, $\alpha_3$ by (A 2) and (A 3) and the definition of $\alpha_i$ $(= -e\sigma_{\max}\lambda_i^{-1}\beta)$. Note that we choose no specific value for the force length parameter $\mu$, since we seek the nature of the first bifurcation point, at bifurcation parameter $h_0$, for different ranges of parameter $\mu$ (this is in contrast to Levy (1995), where the bifurcation parameter was taken to be $\mu$). Thus, based on the solution to (3.7), the bifurcation behaviour may be classified as follows:

$$\left.\begin{aligned} &\mu \in (0.0138, \infty), \quad 1 \text{ (non-symmetrical) root}, \\ &\mu \in (0, 0.0138), \quad 1 \text{ (non-symmetrical)} + 2 \text{ (symmetrical) roots}, \end{aligned}\right\}, \tag{3.10}$$

where the term non-symmetrical root means that a transition to a non-symmetrical equilibrium state will occur for some value of remote load given by (3.8). Alternatively, the term symmetrical root indicates that a bifurcation of equilibrium may occur which retains rotational symmetry. As noted previously, these bifurcations (governed by $\det \boldsymbol{J}_s$) will not occur unless, of course, the inclusion is constrained against rigid displacement. All bifurcation points which initiate from a rotationally symmetric equilibrium state are indicated in (3.10).

Now, in the pre-bifurcated, rotationally symmetric state, cavity shapes are described exactly by circles so we anticipate that only a two term approximation to the separation will be required (i.e. a uniform mode and a non-uniform rigid-body mode). Thus, consider the first two equations in (3.2) which govern the uniform mode multiplier $u_0$ (or $w_0$) and the non-uniform rigid-body mode multiplier u1 (or w1). Because bifurcation will occur when $w_0 = 1$, we introduce variables $\gamma = w_0$, $x = \beta h_0$, $y = w_1$ such that the bifurcation parameter is $w_0$. Then the equations governing $(x, y, \gamma)$ are

$$\begin{aligned} F_1(x, y; \gamma) &= \mu\gamma - x\alpha_0 \mathrm{e}^{-\gamma}[\gamma I_0(y) - y I_1(y)] = 0, \\ F_2(y; \gamma) &= \tfrac{1}{2}\alpha_0 \mathrm{e}^{-\gamma}[-2\gamma I_1(y) + y I_0(y) + y I_2(y)] = 0, \end{aligned} \tag{3.11}$$

where use has been made of (3.2) and (3.4). Uniform equilibrium solutions are of the

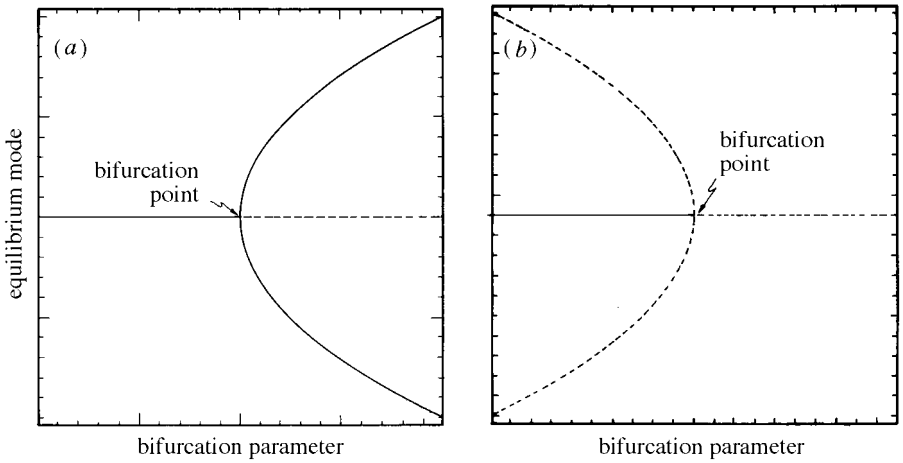


Figure 4. Pitchfork bifurcation. (*a*) Supercritical. (*b*) Subcritical. (Stable equilibrium, solid line; unstable equilibrium, broken line).

form $(\hat{x}, 0; \gamma)$, so that $F_2(y;\gamma) = 0$ is identically satisfied and $F_1(x, y; \gamma) = 0$ results in (3.7 *a*). Now the Jacobian matrix for the system (3.11) can be readily calculated and, when evaluated at the uniform equilibrium $(\hat{x}, 0; \gamma)$, assumes the form

$$\begin{bmatrix} -1 & 0 \\ 0 & -\frac{1}{2}\alpha_0(\gamma - 1)\mathrm{e}^{-\gamma} \end{bmatrix},$$

where the $2\times2$ entry is proportional to $D_{u_0} f$. Thus, at bifurcation $(x, y, \gamma) = (\bar{x}, 0, 1)$, the matrix has a single zero eigenvalue. Because the equation $F_2(y;\gamma) = 0$ governs the bifurcating variable $y$, i.e. it is independent of $x$, it may be analysed separately. Thus, it is easy to show that the following relations hold:

$$F_2(0;1) = 0, \quad \frac{\partial F_2}{\partial y}(0;1) = 0, \quad \frac{\partial F_2}{\partial \gamma}(0;1) = 0, \quad \frac{\partial^2 F_2}{\partial y^2}(0;1) = 0,$$
$$\frac{\partial^2 F_2}{\partial y \partial \gamma}(0;1) = -1, \quad \frac{\partial^3 F_2}{\partial y^3}(0;1) = \tfrac{3}{2},$$

so that the solution undergoes a pitchfork bifurcation (Guckenheimer & Holmes 1983; Wiggins 1990) at $(y;\gamma) = (0;1)$ (or $w_1 = 0$, $w_0 = 1$). Furthermore, because the ratio $-(\partial^3 F_2/\partial y^3(0;1))/(\partial^2 F_2/\partial y \partial \gamma(0;1))$ is positive, the pitchfork is always supercritical, independent of the value of the force length parameter $\mu$ (figure 4*a*). The geometrical meaning of this result is that the non-uniform rigid-body mode multiplier $w_1$ always increases with increasing uniform separation mode multiplier $w_0 > 1$, i.e. after the interface force has attained its maximum value. (Note that stability of equilibria is not assessed according to the sign of the eigenvalues of the Jacobian (of (3.12)) owing to the change of variables used to derive (3.11).

Now shift the bifurcation point $(\bar{x}, 0; \bar{\gamma} = 1)$ to the origin by introducing the variables $u = x - \bar{x}$, $v = y$, and $\rho = \gamma - 1$ and expand (3.11) in a Taylor series about the point $(u, v) = (0, 0)$. The result is given by

$$f(u, v; \rho) = a_0(\rho) - u + a_2(\rho)v^2 + O(4) = 0, \tag{3.12 a}$$
$$g(v; \rho) = b_1(\rho)v + b_3(\rho)v^3 + O(5) = 0, \tag{3.12 b}$$

where the coefficients are given in Appendix C and are such that $a_0(0) = 0$, $a_2(0) =$

$-\frac{1}{4}\alpha_0 e^{-1}$, $b_1(0) = 0$ and $b_3(0) = \frac{1}{8}\alpha_0 e^{-1}$. Now, if terms of order 4 and higher are neglected, solutions to (3.12 *b*) are given by

$$v = y = w_1 = 0, \quad v = y = w_1 = \pm 2\sqrt{2}\sqrt{\frac{\rho}{2-\rho}} = \pm 2\sqrt{2}\sqrt{\frac{w_0 - 1}{3 - w_0}}. \tag{3.13}$$

With the aid of (3.13), solutions to (3.12 *a*) are seen to be of the form

$$u = a_0(\rho), \quad u = a_0(\rho) + a_2(\rho)\left[\frac{8\rho}{2-\rho}\right]. \tag{3.14}$$

Equations (3.13) and (3.14) describe the behaviour of the rigid-body mode multiplier $w_1$, and the load parameter $\beta h_0$, as the uniform mode multiplier $w_0$ increases through the bifurcation point ($w_0 = 1$). In order to understand whether or not the non-symmetrical transition is gradual or abrupt under increasing load we need to construct the function $w_1 : h_0 \to w_1(h_0)$. Thus, eliminate $\rho$ between the second equation in (3.13) and the second equation in (3.14) to obtain

$$u = \tfrac{1}{4}(\mu - \alpha_0 e^{-1})v^2 + O(4),$$

where use has been made of (3.7 *a*). Thus, the equilibrium states are governed by

$$w_1 = \pm\sqrt{\frac{\beta h_0 - \beta \bar{h}_0}{\mu - \alpha_0 e^{-1}}}, \quad w_1 = 0, \tag{3.15}$$

which represents a pitchfork bifurcation at $\beta h_0 = \beta \bar{h}_0$. An inspection of (3.15) indicates that when $\mu > \alpha_0 e^{-1}$, the pitchfork is supercritical (figure 4*a*) and when $\mu < \alpha_0 e^{-1}$, the pitchfork is subcritical (figure 4*b*). This result is significant in that it indicates the parameter values for which the bifurcation at maximum interface force leads to a transition in interfacial separation which is gradual ($\mu > \alpha_0 e^{-1}$) or abrupt ($\mu < \alpha_0 e^{-1}$). That a gradual transition to non-symmetrical equilibrium states occurs when $\mu > \alpha_0 e^{-1}$ is apparent directly from figure 4*a* by noting the stability of the branches emanating from the bifurcation point. When $\mu < \alpha_0 e^{-1}$, however, a rotationally symmetric branch of equilibria meets three unstable branches (two of which yield non-symmetrical states) at the bifurcation point. Thus, it appears that a local analysis of bifurcation is unable to determine behaviour. In § 4, a global analysis is carried out which identifies adjacent stable equilibria so that, for $\mu < \alpha_0 e^{-1}$, an abrupt transition occurs at bifurcation. (For the case of a rigid inclusion, this condition assumes the form $\mu < \beta\sigma_{\max}(1+\nu)/E$.) A further classification of behaviour, based on the two mode approximation is given by

$$\left.\begin{aligned} &\mu \in (0.0377, \infty), \quad \text{1 non-symmetrical bifurcation, supercritical,} \\ &\mu \in (0.0138, 0.0377), \quad \text{1 non-symmetrical bifurcation, subcritical,} \\ &\mu \in (0, 0.0138), \quad \text{1 non-symmetrical} \\ &\qquad\qquad\qquad\qquad +2 \text{ symmetrical bifurcations, subcritical,} \end{aligned}\right\}, \tag{3.16}$$

where supercritical (subcritical) corresponds to the local bifurcation behaviour illustrated in figure 4*a* (figure 4*b*). Note that there are essentially two kinds of behaviour. The first corresponds to gradual non-symmetrical separation after bifurcation (when $\mu \in (0.0377, \infty)$) and the second, to abrupt non-symmetrical separation after bifurcation (when $\mu \in (0, 0.0377)$). If, however, the inclusion is constrained

against rigid displacement, then gradual rotationally symmetric separations occur for $\mu \in (0.0138, \infty)$, while abrupt rotationally symmetric separations will occur for $\mu \in (0, 0.0138)$.

### (*c*) *Tensile load*

Remote uniaxial tension ($S_{11}^{\infty} > 0$, $S_{22}^{\infty} = 0$) is characterized by the parameters $h_0 = (1-\nu^2)S_{11}^{\infty}/E$ and $h_3 = 2h_0$. For this remote load, the displacement jump is non-uniform (but symmetric) in the pre-bifurcated state. Because of this, an additional degree of approximation is involved corresponding to the approximate characterization of the pre-bifurcated state. The simple geometrical condition that bifurcation under equibiaxial load occurs when the interface force attains its maximum value is therefore no longer available for more complex loading.

With $h_3 = 2h_0$, eliminate $h_0$ between (3.3 *a*), (3.3 *b*) to obtain the equation $G(w_0, w_3) = 0$ governing the two symmetric mode multipliers. Thus, consider the system

$$G(w_0, w_3) = \mu(w_0 - \tfrac{1}{2}w_3) + \mathrm{e}^{-w_0}[(\alpha_0 w_0 - \alpha_3 w_3)I_0 + (\alpha_3 + \alpha_3 w_0 - \alpha_0 w_3)I_1] = 0, \tag{3.17 a}$$

$$\det \boldsymbol{J}_s = 0, \tag{3.17 b}$$

$$\det \boldsymbol{J}_u = 0, \tag{3.17 c}$$

where the argument of the modified Bessel functions is $w_3$ and the last two expressions (of (3.17)) are given by (3.5). It is a straightforward matter to solve† (3.17) for those values of $\mu$ for which symmetrical bifurcation may occur (roots to (3.17 *a*) and (3.17 *b*)) and for which non-symmetrical bifurcation may occur (roots to (3.17 *a*) and (3.17 *c*)). In the event that no solution to either (3.17 *a*) and (3.17 *b*), or (3.17 *a*) and (3.17 *c*) can be found, then bifurcation of equilibrium does not occur for those $\mu$ parameter values. Thus we have

$$\left.\begin{aligned} &\mu \in (0.1064, \infty), \quad \text{no roots,} \\ &\mu \in (0.0109, 0.1064), \quad 2 \text{ (non-symmetrical) roots,} \\ &\mu \in (0, 0.0109), \quad 2 \text{ (symmetrical)} + 2 \text{ (non-symmetrical) roots,} \end{aligned}\right\} \tag{3.18}$$

where it is understood that all bifurcation points which initiate from the branch of symmetrical equilibria are indicated at that particular value of $\mu$. In order to determine which bifurcation point will occur first (at a given value of $\mu \in (0, 0.0109)$), we need to compute the corresponding value of $h_0$ for each bifurcation point. This follows directly from (3.3 *a*) (or (3.3 *b*)). In this way it can be demonstrated numerically that non-symmetrical bifurcation always preceeds (i.e. initiates with a lower value of $h_0$) symmetrical bifurcation. The conditions $\det \boldsymbol{J}_s = 0$, $\det \boldsymbol{J}_u = 0$ are, in fact, only necessary conditions for bifurcation and it remains to investigate the detailed character of the transitions which occur at the non-symmetrical bifurcation points described in (3.18).

Consider (3.2) with $h_3 = 2h_0$. Because the necessary condition for bifurcation $\det \boldsymbol{J}_u = 0$ ((3.5 *b*)) is in essence a functional relationship between $w_0$ and $w_3$ (explicitly independent of the remote load) it is convenient to rewrite (3.2) so that (i) the

† Maple Waterloo Software (1994).

bifurcation parameter is $w_0$ and (ii) the determination of $\beta h_0$ is uncoupled from $w_1$, $w_3$. Thus, consider the reduced system

$$f_1(y,z;\gamma) = 0 = \mu(\gamma - \tfrac{1}{2}z) + \frac{1}{2\pi}\int_0^{2\pi} (\alpha_0 - \alpha_3)(\gamma + y\cos\theta + z\cos 2\theta)\mathrm{e}^{-(\gamma + y\cos\theta + z\cos 2\theta)}\,\mathrm{d}\theta,$$

$$f_2(y,z;\gamma) = 0 = \frac{1}{2\pi}\int_0^{2\pi} \alpha_0\cos\theta(\gamma + y\cos\theta + z\cos 2\theta)\mathrm{e}^{-(\gamma + y\cos\theta + z\cos 2\theta)}\,\mathrm{d}\theta, \quad (3.19)$$

where $\gamma = w_0$, $z = w_3$, $y = w_1$ and $x = \beta h_0$ is determined from

$$x = \mu\gamma + \frac{1}{2\pi}\int_0^{2\pi} \alpha_0(\gamma + y\cos\theta + z\cos 2\theta)\mathrm{e}^{-(\gamma + y\cos\theta + z\cos 2\theta)}\,\mathrm{d}\theta. \quad (3.20)$$

An equilibrium solution to system (3.17) is $(y,z) = (0,\hat{z})$, provided

$$f_1(0,\hat{z};\gamma) = \mu(\gamma - \tfrac{1}{2}\hat{z}) + \mathrm{e}^{-\gamma}[(\alpha_0\gamma - \hat{z}\alpha_3)I_0 + (\gamma\alpha_3 - \hat{z}\alpha_0 + \alpha_3)I_1] = 0, \quad (3.21)$$

where use has been made of (3.4) and it is understood that the argument of the Bessel functions is $\hat{z}$. Note that $f_2(0,\hat{z};\gamma) = 0$ identically and $\hat{x}$ follows from

$$\hat{x} = \mu\gamma + \alpha_0\mathrm{e}^{-\gamma}[\gamma I_0 - \hat{z}I_1]. \quad (3.22)$$

Starting from (3.19), it is a straightforward calculation to obtain the Jacobian determinant at the equilibrium $(0,\hat{z})$. As expected, the determinant vanishes when (3.5 *b*) is satisfied or, equivalently, when

$$\gamma(z) = \frac{I_0(z) - zI_0(z) + zI_1(z)}{I_0(z) - I_1(z)}, \quad (3.23)$$

which is a necessary condition for non-symmetrical bifurcation. The equilibrium state $(x,y,z;\gamma) = (\bar{x},0,\bar{z};\bar{\gamma})$ at bifurcation is therefore determined by (3.21)–(3.23). In order to examine the character of the equilibrium solutions near the bifurcation point, we expand (3.19) in a Taylor series about this point retaining terms up to second order. Thus,

$$f_\rho(u,v) = c_0(\rho) + c_1(\rho)u + c_2(\rho)u^2 + c_3(\rho)v^2 + O(3) = 0,$$
$$g_\rho(u,v) = d_1(\rho)v + d_2(\rho)uv + O(3) = 0, \quad (3.24)$$

where

$$u = z - \bar{z} = w_3 - \bar{w}_3, \quad v = y = w_1, \quad \rho = \gamma - \bar{\gamma} = w_0 - \bar{w}_0. \quad (3.25)$$

In a similiar manner, (3.20) can be expanded as well, yielding

$$w = e_0(\rho) + e_1(\rho)u + e_2(\rho)u^2 + e_3(\rho)v^2 + O(3), \quad (3.26)$$

where $w = x - \bar{x} = \beta h_0 = \beta\bar{h}_0$. Note that the $c_i$, $d_i$, $e_i$ coefficients are given in Appendix C. The system (3.24) may be written in the decoupled forms

$$F_\rho(v) = v(\Sigma_0(\rho) + \Sigma_1(\rho)v^2) = 0, \quad (3.27\,a)$$
$$G_\rho(u) = (\Xi_0(\rho) + \Xi_1(\rho)u + \Xi_2(\rho)u^2)(\Xi_3(\rho) + \Xi(\rho)u) = 0, \quad (3.27\,b)$$

where the coefficients in the above equations follow from (3.24) and the expressions for the $c_i$, $d_i$ given in Appendix C. Now these coefficients are complicated functions of the bifurcation point $(\bar{x},\bar{z},\bar{\gamma})$ which, in turn, is obtained from (3.21)–(3.23). In order

to describe the behaviour of solutions of (3.27) qualitatively we need to consider fixed values of force length parameter $\mu$, solve (3.21)–(3.23) for the bifurcation point subject to the data (3.9) and compute the coefficients $c_i$, $d_i$, $e_i$ (as functions of $\rho$). It is not hard to demonstrate computationally that for $\mu \in (0, 0.1064)$, (3.27 *a*) is the generic form for the pitchfork bifurcation since the following criteria are satisfied (Guckenheimer & Holmes 1983; Wiggins 1990):

$$\frac{\partial F_\rho}{\partial v} = 0, \quad \frac{\partial F_\rho}{\partial \rho} = 0, \quad \frac{\partial^2 F_\rho}{\partial v^2} = 0, \quad \frac{\partial F_\rho^2}{\partial \rho \partial v} \neq 0, \quad \frac{\partial^3 F_\rho}{\partial v^3} \neq 0,$$

when evaluated at the bifurcation point $(v, p) = (0, 0)$. Furthermore, (3.27 *b*) is the generic form for the transcritical bifurcation satisfying the following criteria:

$$\frac{\partial G_\rho}{\partial u} = 0, \quad \frac{\partial G_\rho}{\partial \rho}, \quad \frac{\partial^2 G_\rho}{\partial u^2} \neq 0, \quad \frac{\partial G_\rho^2}{\partial \rho \partial v} \neq 0,$$

evaluated at the bifurcation point $(u, \rho) = (0, 0)$. Equilibrium solutions to (3.27) are given by

$$u = \frac{-\Xi_1 - \sqrt{\Xi_1^2 - 4\Xi_0\Xi_2}}{2\Sigma_2}, \quad v = 0, \tag{3.28 a}$$

$$u = -\frac{\Xi_3}{\Xi_4}, \quad v = \pm\sqrt{-\frac{\Sigma_0}{\Sigma_1}}, \tag{3.28 b}$$

where all $\Xi_i$, $\Sigma_i$ are functions of $\rho$ and the negative sign on the radical in (3.28 *a*) has been chosen consistent with $\lim u = 0$, $\rho \downarrow 0$. Note that direct substitution in (3.26) yields $w$ as well. In order to describe the local physical behaviour (predicted by (3.28)) near the bifurcation point we need to know how the uniform symmetrical mode ($w_0 = \gamma = \bar{\gamma} + \rho$), the non-uniform symmetrical mode ($w_3 = z = \bar{z} + u$) and the non-symmetrical rigid-body mode ($w_1 = y = v$) vary under increasing load parameter ($\beta h_0 = x = \bar{x} + w$). First expand (3.29) and $w$ (obtained from (3.26)) in power series about $\rho = 0$ to get

$$u = \Omega_0\rho + O(\rho^2), \quad v = 0, \quad w = \Omega_1\rho + O(\rho^2), \tag{3.29 a}$$

$$u = \Omega_2\rho + O(\rho^2), \quad v = \pm\Omega_3\sqrt{\rho} + O(\rho^{3/2}), \quad w = \Omega_4\rho + O(\rho^2), \tag{3.29 b}$$

where the $\Omega_i$ coefficients are functions of the bifurcation point and are easily calculable once a value of force length parameter $\mu$ is selected. While we expect that the symmetric equilibrium branch given by (3.29 *a*) will be in some sense 'stable' prior to bifurcation ($\beta h_0 < \beta \bar{h}_0$ or $w < 0$), we need to consider the nature of the equilibrium branches just after bifurcation. The two possibilities are that the pitchfork bifurcation of $v$ is supercritical (figure 4*a*), or subcritical (figure 4*b*). If $v$ is regarded as a function of $w$ through the transformations $w : \rho \to \Omega_1\rho$, $w : \rho \to \Omega_4\rho$, then the criteria for super and subcritical bifurcations are $-(\partial^2 F_\rho/\partial v^3)(\mathrm{d}w/\mathrm{d}\rho)/(\partial^2 F_\rho/\partial v \partial\rho) > 0$ or $-(\partial^2 F_\rho/\partial v^3)(\mathrm{d}w/\mathrm{d}\rho)/(\partial^2 F_\rho/\partial v \partial\rho) < 0$, respectively, when evaluated at the bifurcation point. (This distinction will effectively determine when a cavity will form abruptly (subcriticality) or when it will form gradually (supercriticality).) By calculating values of $-(\partial^2 F_\rho/\partial v^3)(\mathrm{d}w/\mathrm{d}\rho)/(\partial^2 F_\rho/\partial v \partial\rho)$ for different values of $\mu$ it can be further demonstrated computationally that for $\mu \in (0.0440, 0.1064)$, the pitchfork is supercritical, while for $\mu \in (0, 0.0440)$, the pitchfork is subcritical. Bifurcation diagrams for the function obtained from (3.29) are given in figure 4*b* for $\mu = 0.01$

and in figure 4*a* for $\mu = 0.05$. Note that Hadamard stability of equilibrium states has been evaluated consistent with the discussion at the end of § 3 *a*.

The classification of behaviour outlined in (3.16) can now be refined, based on the local analysis just described, and is given as

$$\left.\begin{aligned}
&\mu \in (0.1064, \infty), \quad \text{no bifurcations},\\
&\mu \in (0.0440, 0.1064), \quad \text{2 non-symmetrical bifurcations, supercritical},\\
&\mu \in (0.0109, 0.0440), \quad \text{2 non-symmetrical bifurcations, subcritical},\\
&\mu \in (0, 0.0109), \quad \text{2 symmetrical}\\
&\qquad\qquad +\text{2 non-symmetrical bifurcations, subcritical},
\end{aligned}\right\}, \tag{3.30}$$

where the last entry in each row indicates the criticality of the first pitchfork bifurcation. Thus, for $\mu \in (0.1064, \infty)$ (recall that $\mu$ is a measure of the range of action of the force law (2.18)), a symmetric cavity will gradually open under increasing tensile load (ductile decohesion). Within the interval $\mu \in (0.0440, 0.1064)$, bifurcation of the symmetric cavity shape will occur and since the first bifurcation is supercritical, and the non-symmetric branches emanating form the bifurcation point are stable, a non-symmetric cavity will gradually form after bifurcation under increasing tensile load (non-symmetric ductile decohesion). For $\mu \in (0, 0.0440)$, the first bifurcation point reached under increasing tensile load is a non-symmetrical subcritical pitchfork. Because the stable symmetrical branch of equilibria gives way to three unstable branches emanating from the bifurcation point we conjecture that the stable symmetric cavity will abruptly change into a stable non-symmetric cavity (brittle decohesion) at the critical tensile load. In § 4, a global computational analysis of post bifurcation behaviour will be carried out where the classification of behaviour will be further refined. Note that if the inclusion is constrained against rigid displacement, then symmetric bifurcation occurs according to (3.30), i.e. $\mu \in (0, 0.0109)$ for symmetric bifurcation; $\mu \in (0.0109, \infty)$ for no bifurcation.

### (*d*) *Pure shear load*

Consider the remotely applied pure shear loading ($S^{\infty}_{11} = -S^{\infty}_{22}$) characterized by the load parameters $h_0 = 0$, $h_3 = (4(1-\nu^2)/E)S^{\infty}_{11}$. Furthermore, assume the constitutive data given in (3.9). The two term approximation of the symmetrical solution at a prescribed load parameter $h_3$ and force length parameter $\mu$ is readily determined by solving (3.3) for $w_0$, $w_3$. The bifurcation points which initiate from the symmetrical branch of equilibria can be obtained by solving (3.3 *a*) (with $h_0 = 0$), along with $\det \boldsymbol{J}_s = 0$ (for symmetrical bifurcations) and $\det \boldsymbol{J}_u = 0$ (for non-symmetrical bifurcations), where the determinants are given in (3.5). The solutions (Maple Waterloo Software, 1994) indicate that the bifurcation behaviour for varying values of force length parameter $\mu$ is

$$\left.\begin{aligned}
&\mu \in (0.0095, \infty), \quad \text{no roots},\\
&\mu \in (0.0053, 0.0095), \quad \text{2 (symmetrical) roots},\\
&\mu \in (0, 0.0053), \quad \text{2 (symmetrical)} + \text{2(non-symmetrical) roots}.
\end{aligned}\right\} \tag{3.31}$$

An inspection of the analogous results (3.10) (for equibiaxial load) and (3.18) (for tensile load) given in §§ 3 *b* and 3 *c* reveals that there appears to be a qualitative difference in behaviour between the three load cases. First, behaviour under equibiaxial

load differs qualitatively from the other two load cases in that symmetrical ductile decohesion (i.e. no roots) does not occur. Furthermore, roots appear in odd numbers (equibiaxial load) as opposed to even numbers (shear, tension load). (The physical significance of this will be addressed in § 4.) A comparison between behaviour under shear and tensile loading indicates that the values of $\mu$, for which behaviour, other than symmetric ductile decohesion (i.e. no roots), occurs is one order of magnitude smaller for remote shear loading than for remote tensile loading. This is to be expected owing to the additional constraint imposed on the rigid displacement of the inclusion by remote shear loading. Furthermore, under remote shear loading, (3.31) indicates that symmetric ductile decohesion gives way to symmetrical brittle decohesion (two symmetrical roots) under decreasing $\mu$. In contrast, a remote tensile loading precipitates a change from symmetrical ductile decohesion to non-symmetrical ductile decohesion under decreasing $\mu$, as indicated by (3.30). In view of the lack of a valid physical explanation for the response under remote shear loading, we must now consider the 'reasonableness' of characterizing behaviour by a three mode (2 symmetrical + 1 non-symmetrical) approximation.

While it is to be expected that the range of values required for a particular behaviour ((3.31) for remote shear, (3.18) or (3.30) for remote tension and (3.10) or (3.16) for remote equibiaxial load) will change with the number of modes ($n$) in the approximation (2.10), what is not obvious is whether or not the behaviour changes qualitatively with $n$. It has been implicitly assumed so far that the bifurcation behaviour predicted by the two mode approximation for equibiaxial load or the three mode approximation for tensile load coincides with the actual bifurcation behaviour of the system (2.2) and (2.4). This assumption, while true for remote equibiaxial and tensile loading, is generally not true for remote shear loading. In order to see this, consider the five mode approximation (three symmetric modes and two non-symmetric modes) given by (2.10) with $n = 4$. The governing equations (2.9) for this order of approximation are much too complicated to analyse directly according to the local methods of §§ 3 *b* and 3 *c*. They can, however, be integrated numerically by a method to be outlined in § 4. Figures 5 and 6 show bifurcation diagrams for the three mode and the five mode approximation, respectively. In the figures, $u_{\mathrm{s}}$ is the sum of the symmetric modes and $u_{\mathrm{u}}$ is the sum of the non-symmetric modes:

$$u_{\mathrm{s}} = u_0 + \sum_{i=1,2,\ldots} u_{4i-1}, \quad u_{\mathrm{u}} = \sum_{i=1,2,\ldots} u_{4i-3}. \tag{3.32}$$

The load is taken to be a remotely applied shear and the force length parameter $\mu$ is taken to be 0.0075. Figure 5 for the three mode approximation is consistent with (3.31) in that there are two bifurcation points, corresponding to a local maximum and a local minimum, which give rise to symmetric, brittle decohesion as the load parameter $h_3$ is increased. These are tangent bifurcations†. Note that no other branches of equilibria exist and $u_{\mathrm{unsym}} = 0$. The bifurcation diagram for the five mode approximation (figure 6), however, is qualitatively different from the three mode approximation in that it predicts branches of non-symmetric equilibria (parts of which are stable, see § 4). In fact, the behaviour under a remotely applied pure shear will turn out to be qualitatively consistent with the behaviour under a remote tensile load.

† This can be shown formally by the local methods outlined in § 3 *c*.

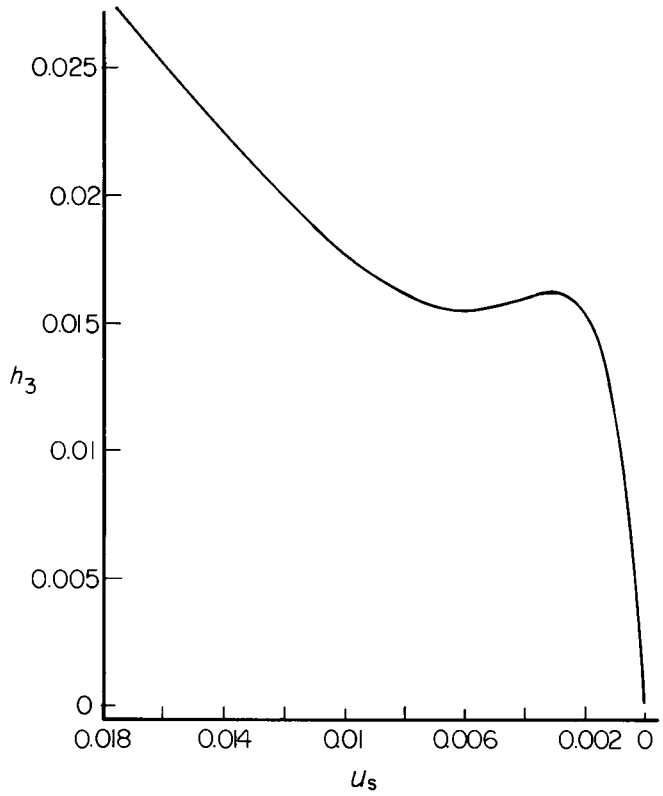


Figure 5. Bifurcation diagram (three mode approximation). Remote shear ($\mu = 0.0075$).

In the following section, a numerical method will be employed to investigate the global bifurcation behaviour of the system as well as the sensitivity of the number of modes ($n$) on behaviour.

## 4. Global bifurcation analysis

In order to determine the stable equilibrium states, or cavity shapes, that occur after bifurcation, a global analysis of behaviour is required. Because the governing equations (2.9) do not admit closed form solutions, a computer program, employing the the Newton–Raphson method together with the composite Simpson $\frac{1}{3}$ rule, was written to solve the system numerically (Press *et al.* 1992). Thus, mode multipliers ($u_i$) are sought for fixed constitutive parameters (3.9), fixed force length ratio $\mu$ and at increasing values of the remote load parameter, $h_0$ or $h_3$, which is incremented in the computations. Non-symmetric solutions ($u_{4i-3}$, $i = 1, 2, \ldots$) are triggered in the calculations by guessing an initial state consistent with the results of local analysis, e.g. (3.28). Typically, the analysis is carried out for a seven mode approximation including four symmetric modes and three non-symmetric modes. Stability of a particular equilibrium is assessed according to the Hadamard criterion by numerical determination of the eigenvalues of the matrix of second partial derivatives of the total potential energy evaluated at the equilibrium. In the following discussion attention is paid to behaviour under remote equibiaxial loading, tensile loading and remote pure shear loading.

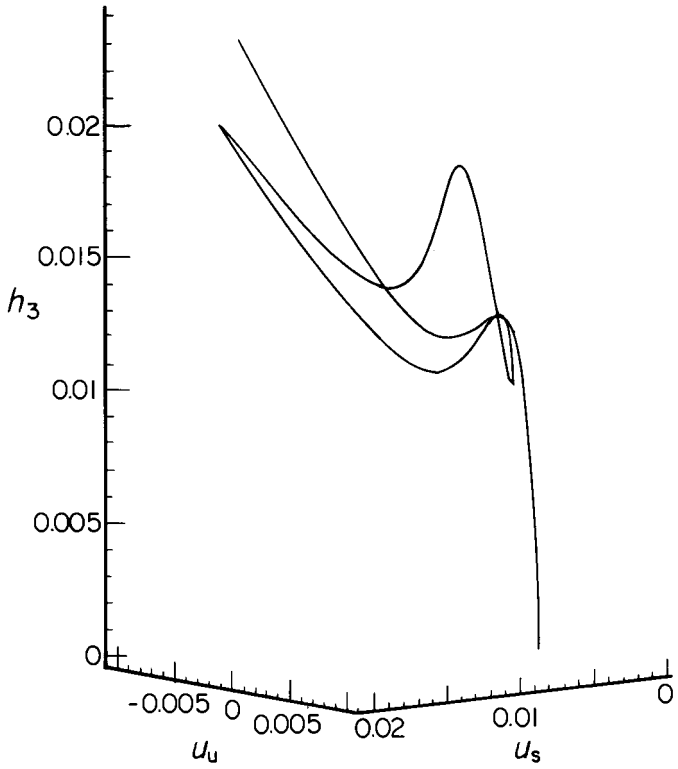


Figure 6. Bifurcation diagram (five mode approximation). Remote shear ($\mu = 0.0075$).

### (*a*) *Equibiaxial load*

Figures 7–9 are three-dimensional bifurcation diagrams of the symmetrical and non-symmetrical mode multipliers $u_s(h_0)$, $u_u(h_0)$ defined by (3.32). The diagrams depict behaviour described in each of the intervals (3.16) obtained from the two mode approximation. (Naturally, these intervals will change owing to the increased accuracy of the seven mode approximation.) Thus, for $\mu = 0.055$, figure 7 indicates that at the bifurcation point (maximum interface force) the stable branch of rotationally symmetric equilibria becomes unstable and there appear two stable branches of non-symmetric (with respect to the $\boldsymbol{e}_2 - \boldsymbol{e}_3$ plane) equilibrium cavity shapes. Under increasing remote load, the inclusion gradually displaces in a rigid manner in a direction which is ultimately dictated by any imperfections in the system. (Note that for the purposes of analysis we have precluded rigid displacement in all but the $\boldsymbol{e}_1$ direction.) The decohesion process at $\mu = 0.055$ is therefore ductile and non-symmetric. The behaviour for parameter value $\mu = 0.030$ is graphically depicted in figure 8. In this case, the stable branch of rotationally symmetric equilibria becomes unstable at bifurcation and two non-symmetric branches are born. The stability of these two branches is such that the parts emanating from the bifurcation point are unstable until tangent bifurcation points are reached whereby the branches become stable. Thus, a transition from a stable rotationally symmetric cavity to a stable non-symmetric cavity cannot be affected continuously and the (rotationally symmetric) cavity changes abruptly, i.e. discontinuously, to a stable adjacent equilibrium state which is non-symmetric. In this instance, decohesion is brittle and non-symmetric. Note that in the two cases just considered the imposition of a constraint of rotational

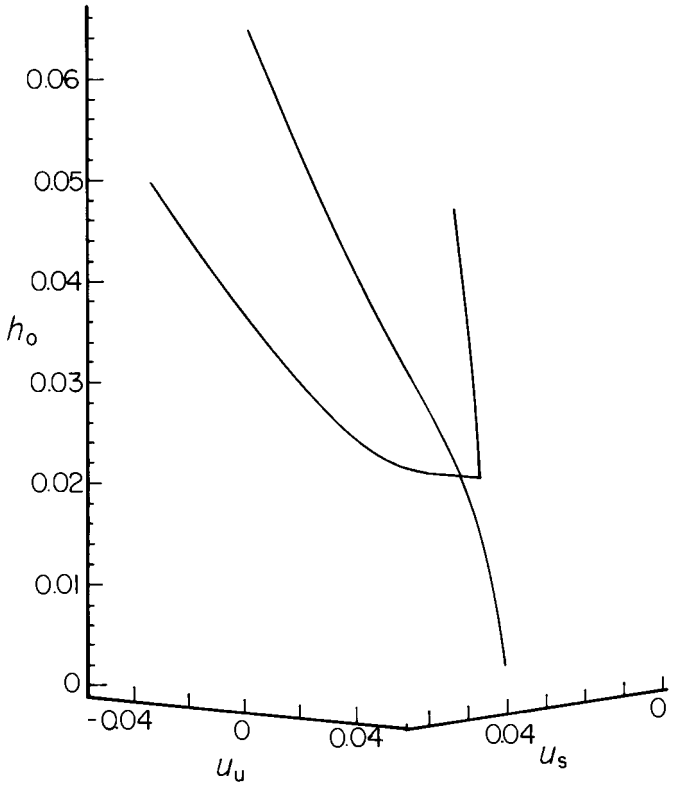


Figure 7. Bifurcation diagram (seven mode approximation). Equibiaxial load ($\mu = 0.055$).

symmetry (i.e. $u_u(h_0) = 0$) renders them to be qualitatively identical in that there then exists one stable branch of rotationally symmetric equilibria and decohesion is ductile. Consider now the behaviour at parameter value $\mu = 0.010$ (figure 9). Qualitatively, the behaviour is similar to the previous one in that rotationally symmetric equilibria give way to the abrupt formation of stable non-symmetric cavities. The difference lies in behaviour, which is constrained to be rotationally symmetric. Unlike the previous two cases, in which one stable branch exists, here, rotationally symmetric bifurcation can occur, i.e. under increasing load, a continuous transition of rotationally symmetric equilibrium states cannot be affected and rotationally symmetric, brittle decohesion occurs.

Values of force length parameter which give rise to a particular type of behaviour were given, for the two mode approximation, by (3.16). The same intervals, for the the seven mode approximation, are

$$\left.\begin{aligned} &\mu \in (0.053, \infty), \quad \text{1 non-symmetrical bifurcation, supercritical,} \\ &\mu \in (0.01, 0.053), \quad \text{1 non-symmetrical bifurcation, subcritical,} \\ &\mu \in (0, 0.014), \quad \text{1 non-symmetrical} \\ &\qquad\qquad\qquad\qquad +\text{2 symmetrical bifurcations, subcritical,} \end{aligned}\right\} \tag{4.1}$$

where the quantitative differences between (3.16) and (4.1) are due to the increased accuracy of the seven mode approximation. Note that the length of the last interval

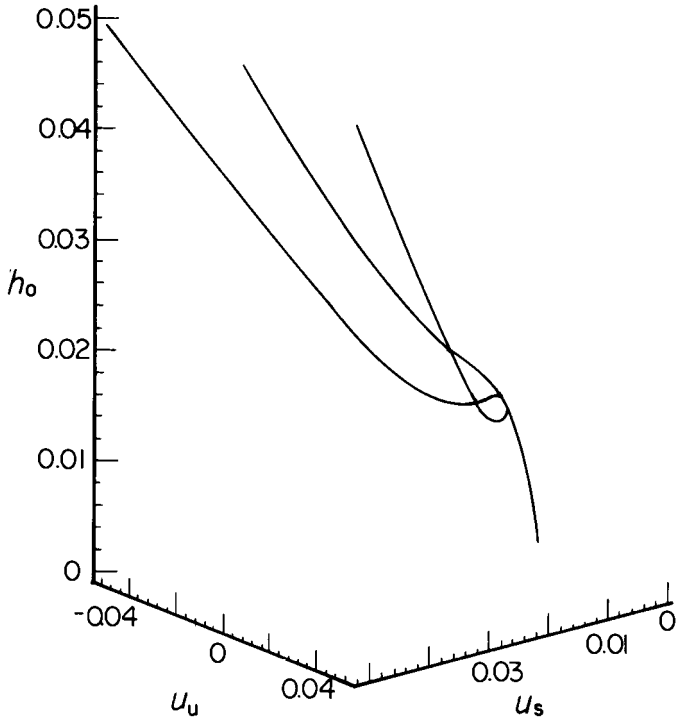


Figure 8. Bifurcation diagram (seven mode approximation). Equibiaxial load ($\mu = 0.030$).

in (3.16) and (4.1) is identical owing to the fact that an exact solution to the pre-bifurcated equilibrium state requires only one uniform mode.

The abrupt, non-symmetric transition, which occurs at load parameter $h_0$ and force length parameter values $\mu \in (0, 0.053)$, is represented pictorially in figures 10*a*,*b*, which depict cavity shapes just before, and just after, bifurcation (at maximum interface force). Because the inclusion is rigid, the normalized (radial) displacement jump $u$ characterizes the displacement of the inner boundary of the matrix so that the (normalized) inner radius (of the matrix) is $r/R : \theta \to 1 + u(\theta)$, where $u$ is given by (2.7). (For the purpose of visualization, the magnitude of the effect has been enhanced by a factor of 5, i.e. the inner radius of the matrix is taken to be $1 + 5u_0 + 5\sum_{i=1}^{6} u_{2i-1} \cos i\theta$ and not $1 + u_0 + \sum_{i=1}^{6} u_{2i-1} \cos i\theta$.) Note that after bifurcation there is significant stretching of the inner boundary of the matrix to accomodate the rigid inclusion (figure 10*b*).

The distribution of interface traction magnitude ($f$) acting on the inclusion surface follows directly from (2.10) and (2.18). For the 7 term approximation it is given by

$$\frac{f}{\sigma_{\max}} = \beta\mu^{-1}\left(u_0 + \sum_{n=1}^{6} u_{2n-1} \cos n\theta\right) \exp\left(1 - \beta\mu^{-1}\left(u_0 + \sum_{n=1}^{6} u_{2n-1} \cos n\theta\right)\right), \quad (4.2)$$

where the coefficients $u_i$ have been obtained numerically. Figure 11 represents the distribution $f$ acting on the inclusion surface just before bifurcation ($h_0 = 0.00987 - O(10^{-6})$) and just after bifurcation ($h_0 = 0.00987 + O(10^{-6})$). At bifurcation the uniform distribution of interface force ($\sigma_{\max}$) gives way to a non-uniform distribution which is such that a large portion of interface is virtually unloaded. There are, however, portions of interface which are subjected to large tensile traction

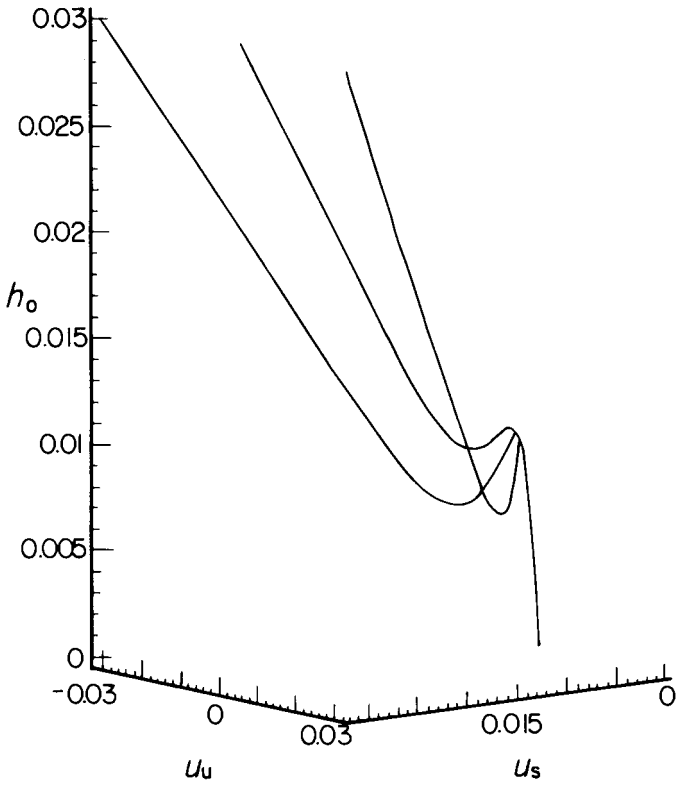


Figure 9. Bifurcation diagram (seven mode approximation). Equibiaxial load ($\mu = 0.010$).

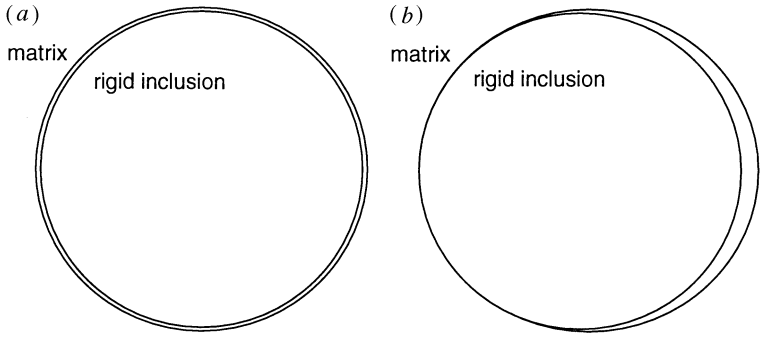


Figure 10. Cavity shapes. ($a$) Just prior to bifurcation at maximum interface force ($h_0 = 0.009\,87 - O(10^{-6})$). ($b$) Just after bifurcation at maximum interface force ($h_0 = 0.009\,87 + O(10^{-6})$) ($\mu = 0.010$).

of magnitude $\sigma_{\max}$ as well as portions which experience compressive traction. The compressive traction corresponds to normal contact forces while the tensile traction corresponds to normal action at a distance forces.

With the mode multipliers $u_i$ known, the circumferential interface displacement jump ($v$) follows by integration (MAPLE 1994):

$$v(\theta) = \sum_{n=1}^{N} v_{2n} \sin n\theta,$$

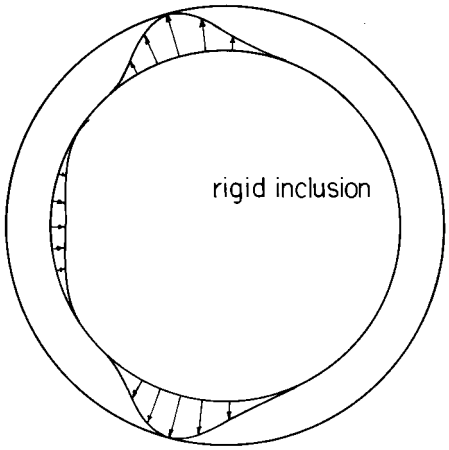


Figure 11. Interface force distribution on a rigid inclusion just before (uniform, $h_0 = 0.009\,87 - O(10^{-6})$) and just after (non-uniform, $h_0 = 0.009\,87 + O(10^{-6})$) bifurcation ($\mu = 0.010$).

where use has been made of (2.16)–(2.18) and the fact that for equibiaxial load $h_\theta(\theta) = 0$. Figure 12 is a graph of $v(\theta)$ for the case where $\mu = 0.01$ and $h_0 = 0.00987 + O(10^{-6})$, i.e. just after bifurcation (see figure 10*b*). In figure 12, $N$ has been taken to be 5. As expected, $v$, which is an odd function of $\theta$, vanishes at $\theta = 0, \pi$.

### (*b*) *Tensile load*

Figures 13–16 are bifurcation diagrams of the symmetrical and non-symmetrical mode multipliers $u_s(h_0)$, $u_u(h_0)$ defined by (3.32). The diagrams depict behaviour described in each of the $\mu$ intervals (3.30) which were obtained from the three mode approximation. Thus, for $\mu = 0.2$, figure 13 indicates that no bifurcations occur and that a stable, symmetric cavity exists for all values of remote load. The decohesion process is therefore symmetrical and ductile. Figure 14 depicts behaviour for $\mu = 0.05$. Here, two non-symmetrical, supercritical bifurcations exist on the symmetrical branch of equilibria. The stability characteristics of the branches indicates that under increasing load the stable, symmetrical cavity gives way to the gradual formation of a stable non-symmetrical cavity. The behaviour is therefore one of non-symmetrical ductile decohesion which, under increasing load, is characterized by the progressive rigid displacement in either direction along the remote load line. According to the figure, this process persists until an equilibrium state is reached whereby the rigid displacement of the inclusion reverses itself and, after some gradual movement, abruptly displaces towards its original symmetrical position at the two symmetrically situated tangent bifurcations. Thereafter, the cavity shapes are all symmetric and occur progressively with increasing load. Figure 15 shows the bifurcation behaviour for the smaller force length parameter $\mu = 0.012$. For this case, there are still two non-symmetrical bifurcations; however, the first is now subcritical. As indicated in the figure, the stability of the branches is such that, under increasing load, a stable symmetric cavity abruptly changes to a stable non-symmetric cavity at the first bifurcation, so the decohesion process is therefore brittle. With further loading the inclusion progressively displaces away from its symmetric state until a (tangent bifurcation) point is reached where the inclusion displacement reverses

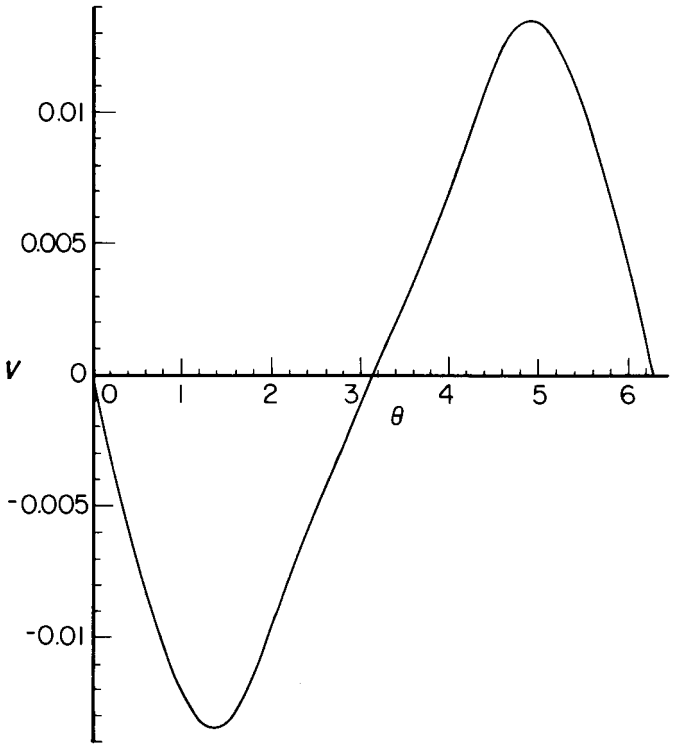


Figure 12. Circumferential interface displacement jump distribution just after bifurcation ($h_0 = 0.009\,87 + O(10^{-6})$) ($\mu = 0.010$).

itself abruptly. Subsequent loading reveals a progressively growing cavity which is symmetric. With a further reduction of interface force length parameter ($\mu$), two additional symmetrical bifurcations appear on the symmetric branch of equilibria consistent with (3.30). Figure 16 illustrates this behaviour for $\mu - 0.005$. Qualitatively, the behaviour is no different from the previous case considered since the two additional (tangent) bifurcations that appear in figure 16 do not affect behaviour. (The first bifurcation reached under increasing load is an abrupt transition from a stable symmetrical cavity to a stable non-symmetric cavity and preceeds the stable but abrupt symmetric cavity to symmetric cavity transition implied by the two additional symmetric bifurcations.) Of course, if the inclusion were constrained against rigid displacement, then the behaviour at $\mu = 0.012$ and $\mu = 0.005$ would be qualitatively different and essentially given by the symmetric branches of figures 13–16. Note that in figure 16 the second non-symmetric bifurcation (on the symmetric branch of equilibria) occurs at a value of load parameter ($h_0$) which is larger than that required for the first non-symmetric bifurcation. With a still further reduction in $\mu$, the bifurcation diagram changes so that the value of $h_0$ at which the second non-symmetric bifurcation occurs is less than that value required for the first (figure 17). For this case, it appears that there are now three (two non-symmetric and one symmetric) stable post bifurcation equilibrium states. Again, owing to the fact that non-symmetric bifurcation initiates first, i.e. at a lower value of $h_0$, it appears that the behaviour is qualitatively the same as that depicted in figures 15 and 16.

The force length parameter intervals required for a given behaviour were given by (3.30) for the three mode approximation. The same intervals for the seven mode

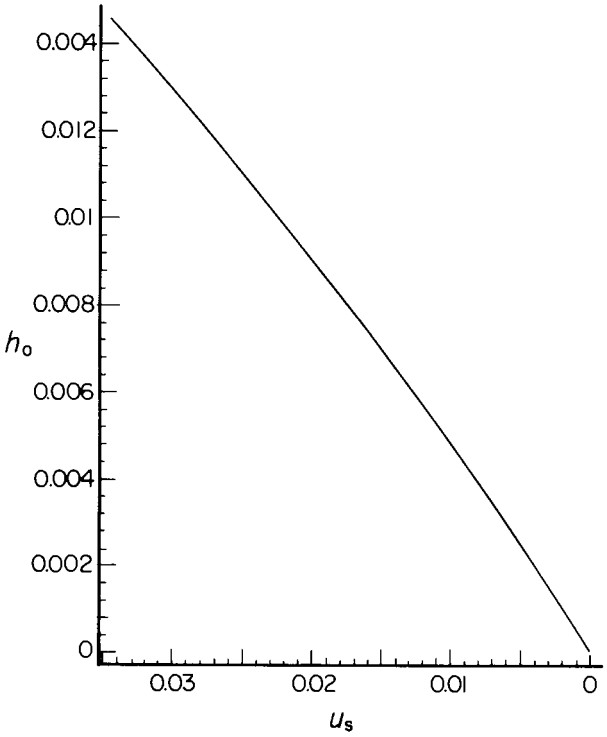


Figure 13. Bifurcation diagram (seven mode approximation). Tensile load ($\mu = 0.200$).

approximation are

$$\left.\begin{aligned}
&\mu \in (0.189, \infty), \quad \text{no bifurcations,}\\
&\mu \in (0.028, 0.189), \quad \text{2 non-symmetrical bifurcations, supercritical,}\\
&\mu \in (0.011, 0.028), \quad \text{2 non-symmetrical bifurcations, subcritical,}\\
&\mu \in (0, 0.011), \quad \text{2 symmetrical}\\
&\qquad\qquad +\text{2 non-symmetrical bifurcations, subcritical.}
\end{aligned}\right\}. \tag{4.3}$$

Obviously, the quantitative differences between (3.30) and (4.3) are due to the more accurate higher approximation. A summary of cavity nucleation under remote tensile load is therefore that, as the force length parameter $\mu$ decreases, the behaviour changes from the gradual formation of symmetric cavities (symmetric, ductile decohesion) to the gradual formation of non-symmetric cavities (non-symmetric, ductile decohesion), followed by the abrupt formation of non-symmetric cavities (non-symmetric, brittle decohesion). In the above description, the transitions initiate from a symmetric cavity shape and occur under increasing load. The behaviour is physically reasonable and consistent with results from the equibiaxial load case in that decreasing $\mu$ tends to make the decohesion process more brittle. Of course, for the tensile load case, symmetric ductile decohesion can occur while this behaviour is absent for equibiaxial loading (i.e. the inclusion must eventually displace rigidly). The somewhat anomalous (and unanticipated) subsequent behaviour of abrupt reversal of rigid displacement towards the symmetric inclusion state (which occurs for three of the force length parameter intervals (4.2)) is more difficult to explain. The fact that it is

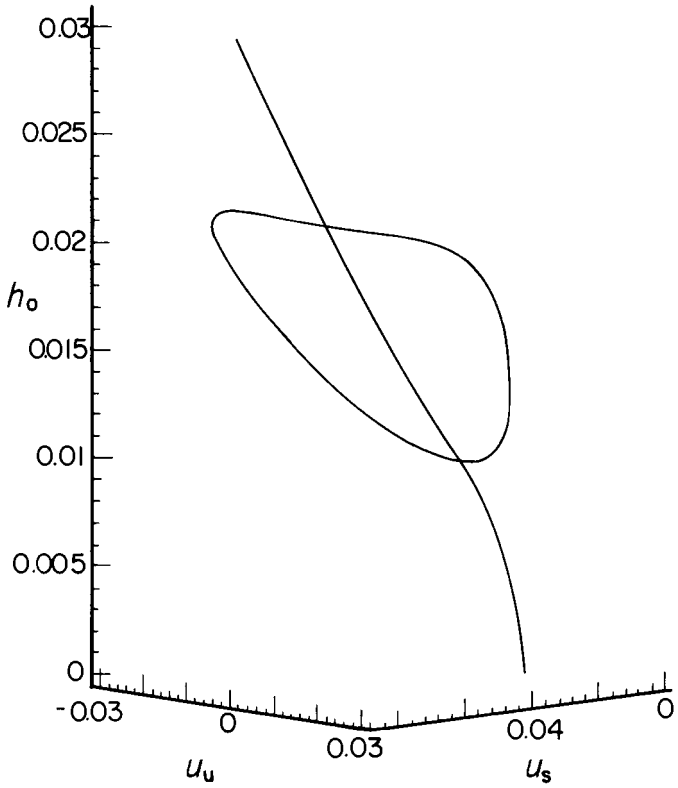


Figure 14. Bifurcation diagram (seven mode approximation). Tensile load ($\mu = 0.050$).

absent in the equibiaxial load case seems to indicate that it is a consequence of the compressive constraint of surrounding material (Poisson effect) normal to the tensile load direction.

Normalized† cavity shapes at various values of remote load and force length parameter $\mu$ are readily obtained (as in § 4 *a*) by graphing the radius of the inner boundary of the matrix. Figures 18 and 19 depict typical cavity shapes for $\mu$ and $h_0$ values of 0.2, 0.015 and 0.05, 0.019, respectively. By (4.3), these are typical equilibrium shapes occuring in a symmetrical (figure 18) or non-symmetrical (figure 19) ductile decohesion process. Note that there is a distortion of the inner boundary of the matrix around the rigid inclusion consistent with the remote tensile loading; however, there is some interpenetration in regions which are roughly 90° to the load line. This is due, in part, to the error incurred in the series approximation of the solution but also to the fact that the interface force law (2.18) allows for relatively small amounts of interpenetration to occur under compressive tractions. The interfacial traction ($f$), for the parameter values of figures 18 and 19, is obtained from (2.18) and figures 20 and 21 show polar plots of $f$ distributed on the inclusion surface. For the symmetrical cavity shape of figure 18, figure 20 indicates that tensile traction acts across the interface gap along the load line while perpendicular to it there is compressive traction which is to be interpreted as a contact traction acting on the inclusion surface. With further increase in applied load, the magnitude of the tensile traction decreases

† With respect to inclusion radius $R$.

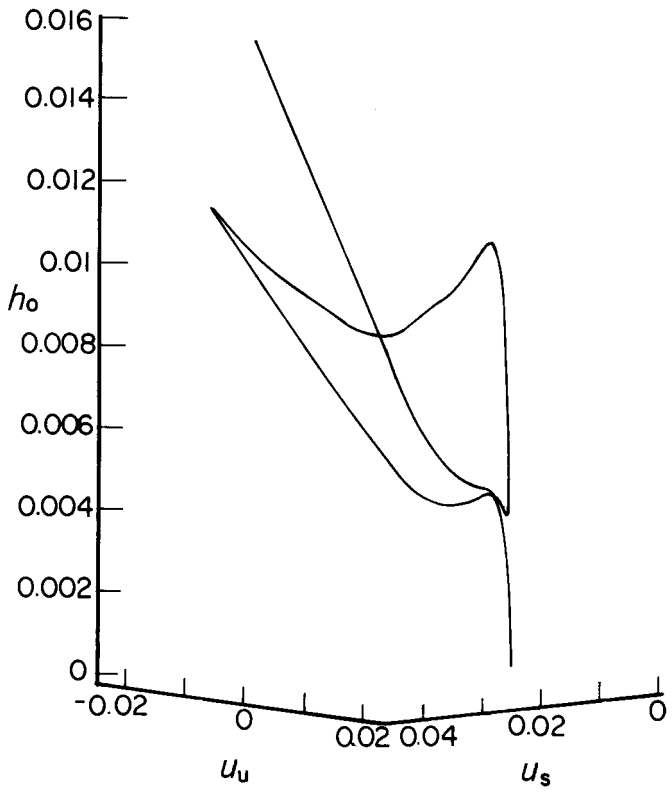


Figure 15. Bifurcation diagram (seven mode approximation). Tensile load ($\mu = 0.012$).

while the contact traction increases as the cavity elongates and distorts around the rigid inclusion. Figure 21 is a plot of $f$ for the (non-symmetric) cavity shape shown in figure 19. Note that the rigid displacement of the inclusion leftward results in virtually no interface force on the right region about the load line. The rest of the inclusion boundary has alternating regions of tensile and compressive loads consistent with equilibrium. Further increase in remote loading causes a void to open up non-symmetrically until a point is reached where the inclusion, in fact, displaces back towards its original position. Upon further loading the inclusion abruptly jumps to this location (figure 22*b* for $h_0 = 0.021\,22 + O(10^{-6})$) from a non-symmetrical state (figure 22*a* for $h_0 = 0.021\,22 - O(10^{-6})$). Figure 23 is a polar plot of the interface force distributions just before and just after this phenomenon. Note that in both states, regions to the left and right of the inclusion are almost completely unloaded while above and below the inclusion centre there are small regions of boundary subject to contact pressures. Further loading results in symmetrical equilibrium states with smaller and smaller regions of contact surface subject to larger and larger pressures. Consider next the parameter value $\mu = 0.012$ which, by (4.3), gives rise to a non-symmetrical, brittle decohesion process. Figures 24*a*,*b* show the stable cavity shapes that exist at virtually identical values of remote load parameter, i.e. figure 24*a* occurs for $h_0 0.004\,17 - O(10^{-6})$, while figure 24*b* occurs for $h_0 = 0.004\,17 + O(10^{-6})$. The figures indicate that the cavity changes abruptly from a small symmetrical shape to a larger non-symmetrical shape formed by the rigid displacement of the inclusion within it. Figure 25 represents a polar plot of the interface force distributions ($f$) for

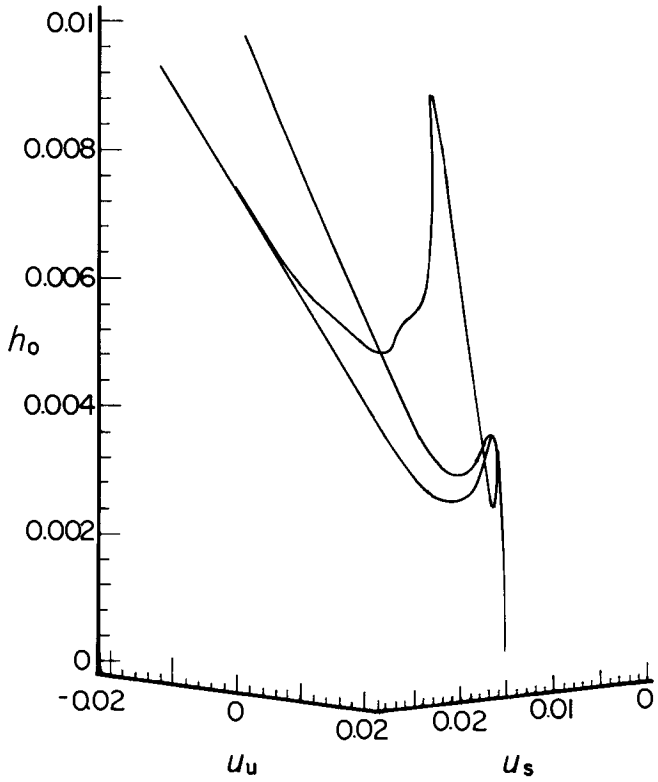


Figure 16. Bifurcation diagram (seven mode approximation). Tensile load ($\mu = 0.005$).

these two cavity shapes. The symmetrical force distribution which occurs just prior to bifurcation has tensile regions right and left along the load line and compressive regions perpendicular to these. Just after bifurcation, the right side of the inclusion near the load line abruptly unloads consistent with the sudden displacement of the inclusion leftward. Further loading results in behaviour described for parameter value $\mu = 0.05$.

The circumferential displacement jump ($v$) can be computed, as for the equibiaxial load case, by direct integration of (2.16)–(2.18). (Note that, for remote tensile loading, the normalized (with respect to inclusion radius) circumferential displacement of the inner boundary of the matrix in the absence of the inclusion is $h_\theta(\theta) = -(2(1-\nu^2)/E)S_{11}^{\infty} \sin 2\theta$.) Now consider $v$ (figure 26) just before and just after non-symmetrical decohesion at the force length parameter value $\mu = 0.012$ and the load parameter $h_0 = 0.004\,17$ (the cavity shapes are shown in figures 24*a*,*b*). As expected, just prior to bifurcation, the distribution of circumferential displacement jump is symmetrical and vanishes at four locations $\theta = 0$, $\frac{1}{2}\pi$, $\pi$ and $\frac{3}{2}\pi$, which are in line with, and perpendicular to, the line of the remote load (figure 26). Just at bifurcation, the circumferential jump abruptly changes such that the zeros perpendicular to the line of the loading shift toward $\theta = \pi$, so as to accomodate the rigid displacement of the inclusion leftward. Furthermore, the magnitude of the jump decreases near the bonded portion of interface and increases near the opposite decohered region (figure 26).

If the sequence of partial sums of the series (2.10) for $u$ converges to a limit function, then the limit function is a solution to (2.2) and (2.4). Alternatively, the con-

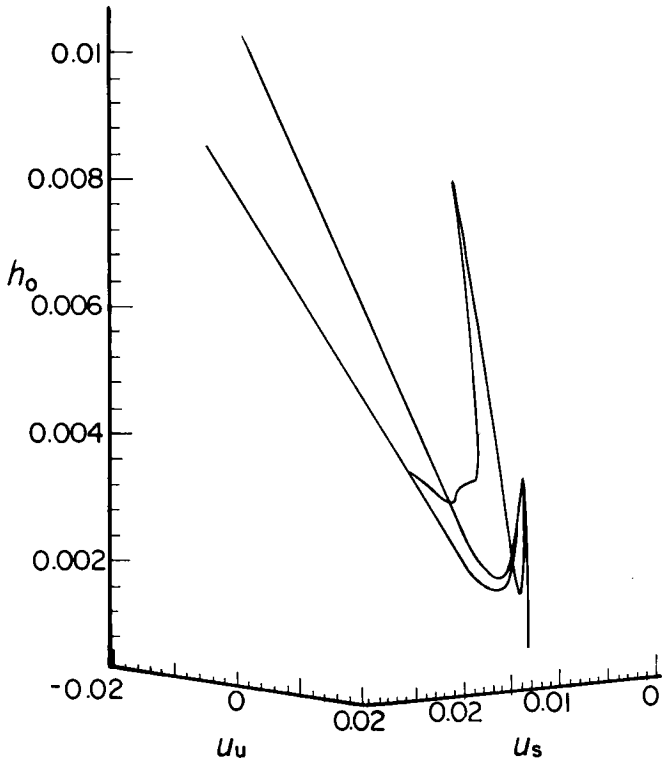


Figure 17. Bifurcation diagram (seven mode approximation). Tensile load ($\mu = 0.002$).

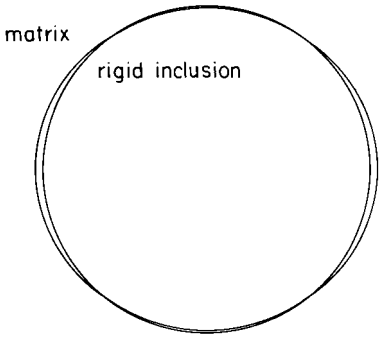


Figure 18. Cavity shape ($h_0 = 0.015$) ($\mu = 0.200$).

vergence of at least a subsequence of the sequence of partial sums of the series (2.10) is guaranteed by Hammerstein's theorem on nonlinear integral equations. Rates of convergence of the mode multipliers $u_i$ can be inferred from a tabulation of the multipliers for various levels of approximation. Thus, table 1 depicts the mode multipliers for the three, four, five, six and seven mode approximations at a force length parameter of $\mu = 0.01$ and a load parameter $h_0 = 0.004\,50$. The table indicates a rapid rate of convergence with the difference between the six and seven mode approximations for the $u_i$ being on the order of 1 part in 100 (for the first four modes). (Recall that (3.30) and (4.3) indicate the qualitative similiarity in behaviour between the three and seven mode approximations.)

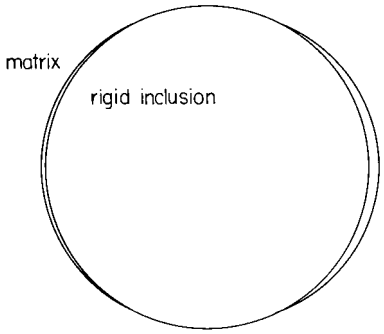


Figure 19. Cavity shape ($h_0 = 0.019$) ($\mu = 0.050$).

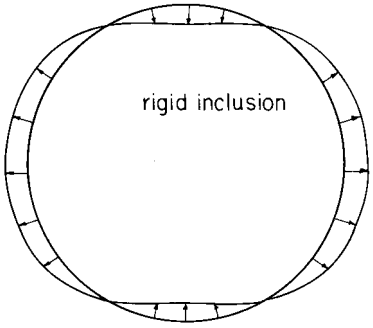


Figure 20. Interface force distribution on a rigid inclusion ($h_0 = 0.015$) ($\mu = 0.200$).

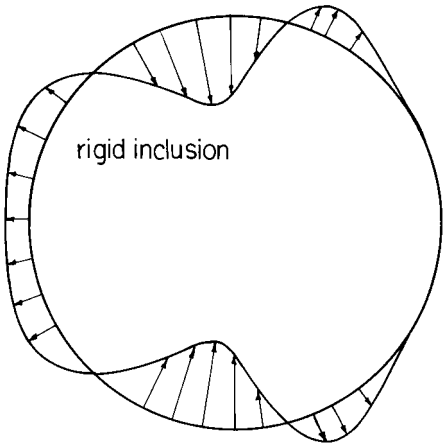


Figure 21. Interface force distribution on a rigid inclusion ($h_0 = 0.019$) ($\mu = 0.050$).

### (*c*) *Pure shear load*

Results for the case where the remote loading is a pure shear are qualitatively the same as those obtained in § 4 *b* (for remote tension loading) and will not be presented graphically. The magnitudes of the intervals of force length parameter $\mu$ which yield a given nucleation behaviour are, however, different from those given in (4.2). Thus,

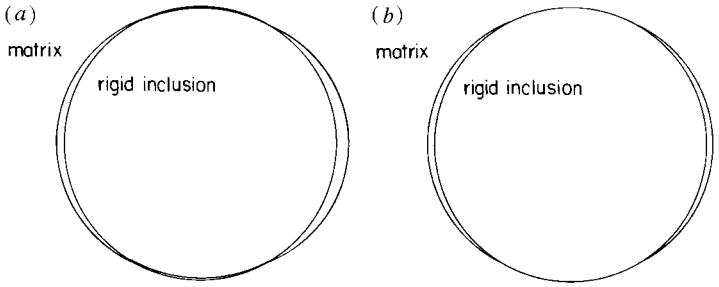


Figure 22. Cavity shapes. (*a*) Unsymmetrical state just prior to bifurcation ($h_0 = 0.02122 - O(10^{-6})$). (*b*) Symmetrical state just after bifurcation ($h_0 = 0.02122 + O(10^{-6})$) ($\mu = 0.050$).

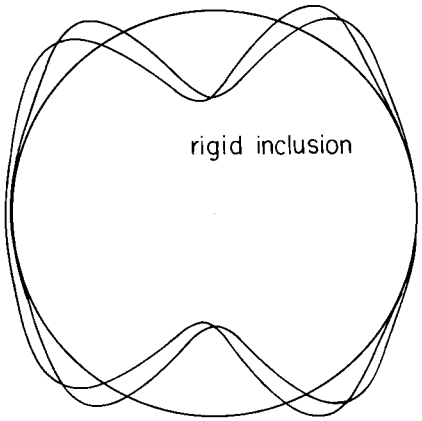


Figure 23. Interface force distribution on a rigid inclusion just before (non-symmetrical, $h_0 = 0.02122 - O(10^{-6})$) and just after (symmetrical, $h_0 = 0.02122 + O(10^{-6})$) bifurcation ($\mu = 0.050$).

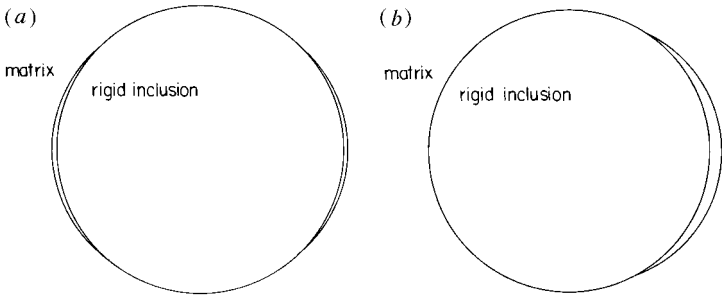


Figure 24. Cavity shapes. (*a*) Symmetrical state just prior to bifurcation ($h_0 = 0.00417 - O(10^{-6})$). (*b*) Unsymmetrical state just after bifurcation ($h_0 = 0.00417 + O(10^{-6})$) ($\mu = 0.012$).

for remote shear, there is

$$\left.\begin{array}{ll} \mu \in (0.029, \infty), & \text{no bifurcations,} \\ \mu \in (0.018, 0.029), & \text{2 non-symmetrical bifurcations, supercritical,} \\ \mu \in (0.009, 0.018), & \text{2 non-symmetrical bifurcations, subcritical,} \\ \mu \in (0, 0.009), & \text{2 symmetrical} \\ & \quad +\text{2 non-symmetrical bifurcations, subcritical.} \end{array}\right\}. \tag{4.4}$$

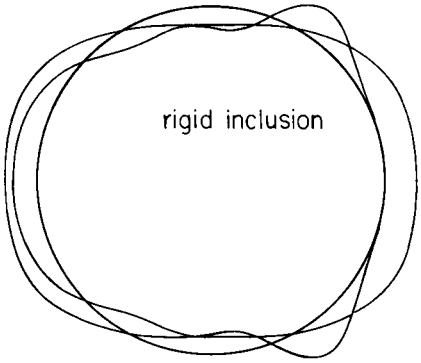


Figure 25. Interface force distribution on a rigid inclusion just before (symmetrical, $h_0 = 0.004\,17 - O(10^{-6})$) and just after (non-symmetrical, $h_0 = 0.004\,17 + O(10^{-6})$) bifurcation ($\mu = 0.012$).

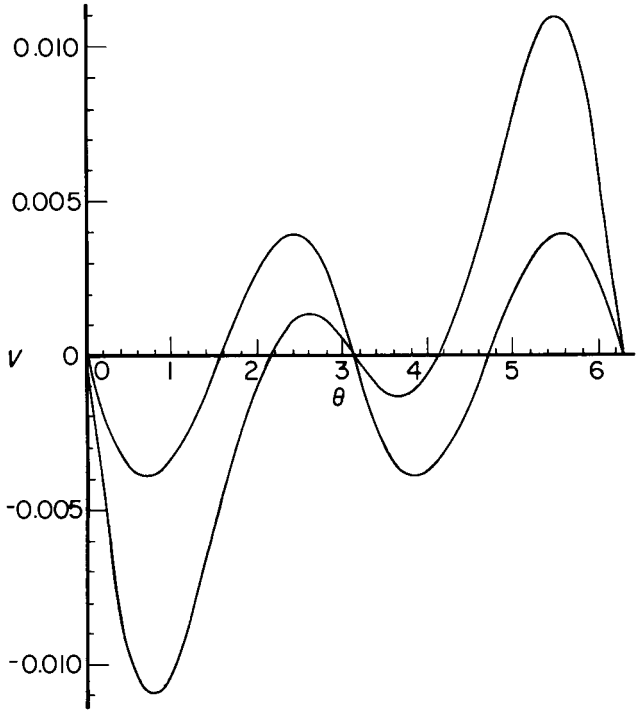


Figure 26. Circumferential interface displacement jump distribution just before ($h_0 = 0.004\,17 - O(10^{-6})$) and just after ($h_0 = 0.004\,17 + O(10^{-6})$) bifurcation ($\mu = 0.012$).

By comparison with (4.3), it is apparent that the window of parameter values ($\mu$), for which either gradual or abrupt non-symmetrical decohesion occurs, is smaller for remote shear than for remote tensile loading. That is, for remote shear, the interface force ($f$) would have to act over a shorter range in order for bifurcation to occur owing to the additional constraint due to the remote compressive stress which, together with remote tension, comprises shear loading. Another aspect of behaviour is the fact that, under remote tension, the window of $\mu$ values which give rise to non-symmetrical, ductile decohesion is larger then the window which yields non-symmetrical, brittle decohesion. When the remote loading is a pure shear this is

Table 1. *Convergence of mode multipliers; remote tension*
($m = 0.01$, $h_0 = 0.0045$.)

| $n$ | $u_0$ | $u_1$ | $u_3$ | $u_5$ | $u_7$ | $u_9$ | $u_{11}$ |
|---|---|---|---|---|---|---|---|
| 3 | 0.004 36 | 0.006 21 | 0.004 31 | | | | |
| 4 | 0.004 65 | 0.007 97 | 0.005 43 | 0.001 92 | | | |
| 5 | 0.004 28 | 0.007 45 | 0.005 59 | 0.002 32 | 0.000 72 | | |
| 6 | 0.004 43 | 0.007 67 | 0.005 65 | 0.002 21 | 0.000 58 | −0.000 21 | |
| 7 | 0.004 46 | 0.007 77 | 0.005 71 | 0.002 24 | 0.000 47 | −0.000 32 | −0.000 31 |

reversed with the larger window of parameter values being that which gives rise to brittle, non-symmetrical behaviour. Of course, overall, the window of $\mu$ values for a given behaviour are smaller for shear then for tensile loading. Note that the behaviour described by (4.4) is not consistent with the predictions of the local analysis (based on the three mode approximation) carried out in § 3 *d*, i.e.

$$\left.\begin{aligned} &\mu \in (0.0095, \infty), \quad \text{no bifurcations,} \\ &\mu \in (0.0053, 0.0095), \quad \text{2 symmetrical bifurcations,} \\ &\mu \in (0, 0.0053), \quad \text{2 symmetrical + non-symmetrical bifurcations.} \end{aligned}\right\} \tag{4.5}$$

This fact was noted in § 3 *d* as well, where the results of the three mode approximation were compared with a numerical calculation of behaviour for the five mode approximation. The consistency of behaviour for the four (not shown) five, six (not shown) and seven mode approximations indicate that for remote shear, at least four modes are required for a correct qualitative prediction.

## 5. Concluding remarks

The viewpoint adopted in this paper has been that cavity nucleation, and the various phenomena associated with it, is a process that occurs naturally through the interaction of remote load, elastic matrix and inclusion and nonlinear interface force–interface separation mechanism. Because the analysis employs no *ad hoc* assumptions concerning nucleation, further assessment of the predictions of the classical nucleation criteria, begun in the Introduction, may now be given against those presented in the preceeding sections. To this end, reconsider the case of a rigid inhomogeneity embedded in an unbounded matrix subject to a remote equibiaxial load (figure 1). Recall that the critical interfacial stress criterion yields the value $S_{\mathrm{S}}^*$ (given by (1.1)) for the remote load required for 'nucleation'. (It has been noted previously (§ 1) that the precise meaning of the term nucleation in the critical stress criterion is never explicitly stated.) Now condition (3.8) relates the physical and geometrical parameters at bifurcation, i.e. at the maximum value of the interface force. For the rigid inhomogeneity, (3.8) may be written as

$$S^* = \frac{\sigma_{\max}}{2(1-\nu)} + \frac{\beta^{-1}\mu E}{2(1-\mu^2)}. \tag{5.1}$$

If the interface is regarded as rigidly bonded, i.e. there is no interfacial separation prior to the attainment of $S^*$, then $\mu \downarrow 0$ (figure 3) and, as required, $S^* \downarrow S_{\mathrm{S}}^*$.

(Note that (3.7 *a*) and (3.7 *c*) imply that when $\mu \downarrow 0$ the critical load for rotationally symmetric bifurcation is also $\sigma_{\max}/(2(1-\nu))$.) Because the event that occurs with the satisfaction of $S = S^*$ for small $m$ is abrupt (brittle) non-symmetrical decohesion (see (3.16)), a comparison of $S^*$ with the critical interfacial stress criterion $S_{\mathrm{S}}^*$ (given by (1.1)) indicates that $S_{\mathrm{S}}^*$ underestimates the remote stress required for this behaviour; the magnitude of the error being worse for longer range forces and smaller inclusion radii (recall $\mu = \delta/R$). It appears then, that the critical interfacial stress criterion gives a reasonable prediction of the onset of brittle non-symmetrical decohesion when the interfacial force is short range. (Note that the critical event is the abrupt rigid displacement of the inhomogeneity within a suddenly larger cavity.) For longer range forces (larger $\mu$), the criterion is virtually meaningless since no critical event (such as brittle decohesion) occurs when $S = S_{\mathrm{S}}^*$ (see (3.16)). In fact, it is (5.1), and not (1.1), which governs the transition from the gradual formation of rotationally symmetric cavities to the gradual development of non-symmetric cavities.

When the remote load is uniaxial, tension interfacial traction is distributed non-uniformly along the interface. The critical interfacial stress criterion implies that when (1.3) is satisfied, i.e. the interface strength is attained at $\theta = 0, \pi$, a cavity 'nucleates'. This criterion cannot be valid, even in the limit of a coherent interface ($\mu \downarrow 0$), because no critical event is associated with it. This follows from the fact that bifurcation is governed by the vanishing of the determinants (2.13) and (2.14). These relations constrain the distribution of slope of the interface force law at bifurcation but are not equivalent to simply requiring a zero slope at the points $\theta = 0, \pi$.

It is obvious that the basic mechanisms by which cavities nucleate will be strongly influenced by both the constitutive characteristics of the matrix and interface, and the interaction effects of neighbouring inclusions. In this regard, the effects of non-linear matrix material behaviour and interfacial friction, neither of which is included in this paper yet both of which occur in real materials, will need to be considered in future work. The incorporation of matrix plasticity in the framework presented in this paper can be expected to yield formidable mathematical difficulties. The incorporation of frictional effects at the interface can be expected to lead to a more mathematically tractable problem; however, the difficulty would be in choosing an appropriate form of the tangential force–tangential separation relation which is sufficiently general. The effects of inclusion–inclusion interaction on the formation of cavities can be expected to be severe in situations of practical interest; that is, inclusions which are added to the matrix in non-dilute concentration so as to realize improved aggregate properties. Solutions of the type described in this paper may be used as building blocks to construct overall effective moduli of an aggregate consisting of inclusions which decohere from the matrix according to interface force law (2.18). While the effective medium models employing these 'solitary defect' solutions are in a sense approximate they can be used to give a qualitative picture of aggregate behaviour. (An analysis of the effective transverse bulk modulus of a composite whose fibres decohere according to force law (2.18), and which implements solitary inclusion solutions of the kind described here, is given in Levy (1996).)

Finally, while the analysis described in this paper assumes that cavity nucleation is in essence an infinitesimal strain phenomenon†, an extensive literature exists (largely

† Although cavities have been observed in material subject to small overall straining (Rogers 1960; Hahn & Rosenfield 1966; Cox & Low 1974; Nutt & Needleman 1987), this fact does not necessarily guarantee the validity of an infinitesimal strain framework.

beginning with the work of Ball (1982)) which treats cavitation within the framework of finite strain elasticity. In these theories, cavitation is not caused by stress concentrators but by a fundamental material instability, the existence of which hinges on the nonlinear kinematics inherent in a finite strain formulation. Depending on the constitutive characteristics of the material and the geometry of the solid (e.g. uniform or composite sphere or cylinder), a variety of behaviours can occur ranging from gradual to abrupt formation of radially symmetric (or possibly non-symmetric) cavities. For a general review of research on this problem, see Horgan & Polignone (1995).

## Appendix A. Kernels $K_r$, $K_\theta$ and inhomogeneous terms $h_r, h_\theta$

The terms $K_r$, $K_\theta$, $h_r$ and $h_\theta$ appearing in (2.2) and (2.3) have been presented in Levy (1991). The kernel $K_r$ is symmetric and weakly singular with the form

$$K_r = \frac{1-\nu^{*2}}{\pi E^*} + \left[\frac{1-\nu^2}{\pi E} + \frac{1-\nu^{*2}}{\pi E^*}\right]\cos(\theta-\theta')\log(1-\cos(\theta-\theta')) + \Phi(\theta-\theta')\sin(\theta-\theta'),$$

where $\Phi(\theta)$ is $2\pi$ periodic and odd in $\phi$, i.e. for $0 < \phi < 2\pi$, $2\pi\Phi = [(1+\nu)(1-2\nu)/E - (1+\nu^*)(1-\nu^*)/E^*](\pi-\phi)$. $K_r$ has a mean convergent Fourier expansion given by the bilinear formula for weakly singular kernels (Mikhlin 1960):

$$K_r(\theta-\theta') = \sum_{i=1}^{\infty} \frac{\varphi_i(\theta)\varphi(\theta')}{\lambda_i}, \tag{A 1}$$

with eigenvalues

$$\lambda_0 = \frac{-EE^*}{(1+\nu^*)(1-2\nu^*)E + (1+\nu)E^*}, \tag{A 2}$$

$$\lambda_{2n-1} = \lambda_{2n} = \frac{-(n^2-1)EE^*}{2n[(1-\nu^{*2})E + (1-\nu^2)E^*] + (1+\nu)(1-2\nu)E^* - (1+\nu^*)(1-2\nu^*)E}, \quad n = 2,3,\ldots \tag{A 3}$$

and eigenfunctions

$$\varphi_0 = \frac{1}{\sqrt{2\pi}}, \quad \varphi_{2n-1} = \frac{\cos n\theta}{\sqrt{\pi}}, \quad \varphi_{2n} = \frac{\sin n\theta}{\sqrt{\pi}}, \quad n = 2,3,\ldots \tag{A 4}$$

Furthermore, the kernel $K_\theta$ takes the form

$$K_\theta = -\left[\frac{1-\nu^2}{\pi E} + \frac{1-\nu^{*2}}{\pi E^*}\right]\sin(\theta-\theta')\log(1-\cos(\theta-\theta')) + \Phi(\theta-\theta')\cos(\theta-\theta')$$

and has a mean convergent Fourier expansion

$$K_\theta = \sum_{n=2}^{\infty}\left\{\left[\frac{2(1-\nu^2)}{E} + \frac{2(1-\nu^{*2})}{E^*}\right] + \left[\frac{(1+\nu)(1-2\nu)}{E} - \frac{(1+\nu^*)(1-2\nu^*)}{E^*}\right]n\right\} \times \frac{\varphi_{2n}(\theta)\varphi_{2n-1}(\theta') - \varphi_{2n-1}(\theta)\varphi_{2n}(\theta')}{n^2-1}. \tag{A 5}$$

Note that the expansions for $K_r$ and $K_\theta$ do not have terms proportional to $\sin\theta$ and $\cos\theta$. This is due to the constraint of rigid-body equilibrium of the inclusion

characterized by (2.4) in integral equations (2.2) and (2.3). Finally, it has been shown (Levy 1991) that, for remote equibiaxial loading, the inhomogeneous terms ($h_r$, $h_\theta$) in (2.2) and (2.3) assume the forms

$$h_r(\theta) = \frac{1-\nu^2}{E}[(S_{11}^\infty + S_{22}^\infty) + 2(S_{11}^\infty - S_{22}^\infty)\cos 2\theta] = h_0 + h_3 \cos 2\theta,$$
$$h_\theta(\theta) = \frac{2(1-\nu^2)}{E}(S_{11}^\infty - S_{22}^\infty)\sin 2\theta. \tag{A 6}$$

## Appendix B. The demonstration that the $I_{ij} - \int_0^{2\pi} \Gamma(\theta)\cos i\theta \cos j\theta \,\mathrm{d}\theta$, with $\Gamma(\theta) = \Gamma(\theta+\pi)$, satisfy equation (B 1)

$$I_{ij} = \begin{cases} 0, & i \text{ odd (even)}, j \text{ even (odd)}, \\ 2\displaystyle\int_0^\pi \Gamma(\theta)\cos i\theta \cos j\theta \,\mathrm{d}\theta, & i, j \text{ odd or } i, j \text{ even}. \end{cases} \tag{B 1}$$

Let $\Gamma(\theta)$ be a continuous and bounded function such that $\Gamma(\theta) = \Gamma(\theta+\pi)$. For $i$, $j$ fixed, split $I_{ij}$ into two integrals $I_{ij}^{\mathrm{a}}$, $I_{ij}^{\mathrm{b}}$ over the subdomains $(0,\pi)$ and $(\pi, 2\pi)$, respectively. Now change the variable of integration in $I_{ij}^{\mathrm{b}}$ according to $\phi = \theta - \pi$ and note that $\cos i(\phi+\pi) = (-1)^i \cos i\phi$. Then $I_{ij}^{\mathrm{b}} = (-1)^i(-1)^j I_{ij}^{\mathrm{a}}$ and the sum $I_{ij} = I_{ij}^{\mathrm{a}} + I_{ij}^{\mathrm{b}}$ is $(1+(-1)^i(-1)^j)I_{ij}^{\mathrm{a}}$, which demonstrates the assertion.

In order to show that (2.9 *b*) and (2.9 *d*) (with $j$ odd) are identically satisfied for symmetrical solutions $u(\theta)$, let $\Gamma(\theta) = f(u(\theta))$, with $u(\theta) = u_0 + \sum_{i=1}^n u_{2i-1}\cos i\theta$. Now, symmetrical solutions $u(\theta)$ require that $u_{2k-1} = 0$, $k = 1, 3, \ldots$, so that $\Gamma(\theta) = \Gamma(\theta+\pi)$. Then the result follows directly from $I_{ij} = (1+(-1)^i(-1)^j)I_{ij}^{\mathrm{a}}$ by letting $i = 0$ and $j = 1, 3, \ldots$

## Appendix C. The coefficients $a_i$, $b_i$, $c_i$, $d_i$ and $e_i$

The coefficients $a_0$, $a_2$, $b_1$, $b_3$ appearing in (3.12) have the form

$$a_0(\rho) = -\hat{x} + (1+\rho)(\mu + \alpha_0 \mathrm{e}^{-(1+\rho)}),$$
$$a_2(\rho) = -\tfrac{1}{4}\alpha_0 \mathrm{e}^{-(1+\rho)}(1-\rho),$$
$$b_0(\rho) = -\tfrac{1}{2}\alpha_0 \mathrm{e}^{-(1+\rho)}\rho,$$
$$b_3(\rho) = \tfrac{1}{16}\alpha_0 \mathrm{e}^{-(1+\rho)}(2-\rho).$$

The coefficients appearing in (3.24) and (3.26) are of the form

$$\begin{aligned} c_0(\rho) = {} & \mu\rho + \mathrm{e}^{-(\bar\gamma+\rho)}[(\alpha_0\bar\gamma + \alpha_0\rho - \bar{x}\alpha_3)I_0(\bar{x}) + (\alpha_3 + \alpha_3\rho + \alpha_3\bar\gamma - \bar{x}\alpha_0)I_1(\bar{x})] \\ & - \mathrm{e}^{-\bar\gamma}[(\alpha_0\bar\gamma - \bar{x}\alpha_3)I_0(\bar{x}) + (\alpha_3 + \alpha_3\bar\gamma - \bar{x}\alpha_0)I_1(\bar{x})], \\ c_1(\rho) = {} & -\tfrac{1}{2}\mu - \mathrm{e}^{-(\bar\gamma+\rho)}[(\alpha_0\bar{x} + \alpha_3 - \alpha_3\bar\gamma - \alpha_3\rho)I_0(\bar{x}) \\ & + (-\alpha_0\rho - \alpha_0\bar\gamma + \alpha_3\rho\bar{x}^{-1} + \alpha_3\bar{x}^{-1} + \tfrac{3}{4}\alpha_3\bar{x})I_1(\bar{x}) + \tfrac{1}{4}\alpha_3\bar{x}I_3(\bar{x})], \\ c_2(\rho) = {} & -\mathrm{e}^{-(\bar\gamma+\rho)}[(\tfrac{1}{2}\alpha_0 - \tfrac{1}{4}\alpha_0\bar\gamma - \tfrac{1}{4}\alpha_0\rho + \tfrac{3}{16}\bar{x}\alpha_3)I_0(\bar{x}) \\ & + (\tfrac{3}{8}\alpha_0\bar{x} - \tfrac{3}{8}\alpha_3\rho - \tfrac{3}{8}\alpha_3\bar\gamma + \tfrac{3}{4}\alpha_3)I_1(\bar{x}) + (\tfrac{1}{2}\alpha_0 - \tfrac{1}{4}\alpha_0\bar\gamma - \tfrac{1}{4}\alpha_0\rho + \tfrac{1}{4}\alpha_3\bar{x})I_2(\bar{x}) \\ & + (\tfrac{1}{8}\alpha_0\bar{x} - \tfrac{1}{8}\alpha_3\rho - \tfrac{1}{8}\alpha_3\bar\gamma + \tfrac{1}{4}\alpha_3)I_3(\bar{x}) + \tfrac{1}{16}\bar{x}\alpha_3 I_4(\bar{x})], \end{aligned}$$

$$
\begin{aligned}
c_3(\rho) &= -\mathrm{e}^{-(\bar\gamma+\rho)} \\
&\quad \times[(\tfrac{1}{2}\alpha_0 - \tfrac{1}{4}\alpha_0\bar\gamma - \tfrac{1}{4}\alpha_0\rho - \tfrac{1}{8}\bar x\alpha_0 - \tfrac{1}{4}\alpha_3 + \tfrac{1}{8}\bar\gamma\alpha_3 \\
&\quad +\tfrac{1}{8}\bar\gamma\alpha_3 + \tfrac{1}{8}\rho\alpha_3 + \tfrac{1}{8}\bar x\alpha_3)I_0(\bar x) \\
&\quad -(\tfrac{1}{2}\alpha_0 - \tfrac{1}{4}\alpha_0\bar\gamma - \tfrac{1}{4}\alpha_0\rho - \tfrac{1}{4}\bar x\alpha_0 - \tfrac{1}{2}\alpha_3 + \tfrac{1}{4}\bar\gamma\alpha_3 + \tfrac{1}{4}\rho\alpha_3 + \tfrac{3}{16}\bar x\alpha_3)I_1(\bar x) \\
&\quad +(-\tfrac{1}{8}\bar x\alpha_0 - \tfrac{1}{4}\alpha_3 + \tfrac{1}{8}\bar\gamma\alpha_3 + \tfrac{1}{8}\rho\alpha_3 + \tfrac{1}{8}\bar x\alpha_3)I_2(\bar x) - \tfrac{1}{16}\bar x\alpha_3 I_3(\bar x)], \\
d_1(\rho) &= \tfrac{1}{2}\alpha_0\mathrm{e}^{-(\bar\gamma+\rho)}[(1-\bar\gamma-\rho\bar x)I_0(\bar x) + (\bar\gamma+\rho+\bar x)I_1(\bar x)], \\
d_2(\rho) &= -\tfrac{1}{2}\alpha_0\mathrm{e}^{-(\bar\gamma+\rho)}[(1-\tfrac{1}{2}\bar\gamma - \tfrac{1}{2}\rho - \tfrac{1}{2}\bar x)I_0(\bar x) - (2-\bar\gamma-\rho+\tfrac{3}{4}\bar x)I_1(\bar x) \\
&\quad +(1-\tfrac{1}{2}\bar\gamma - \tfrac{1}{2}\rho - \tfrac{1}{2}\bar x)I_2(\bar x) - \tfrac{1}{4}\bar x I_3(\bar x)], \\
e_0(\rho) &= \mu\rho + \mathrm{e}^{-(\bar\gamma+\rho)}[(\alpha_0\bar\gamma + \alpha_0\rho)I_0(\bar x) - \bar x\alpha_0 I_1(\bar x)] - \mathrm{e}^{-\bar\gamma}[\alpha_0\bar\gamma I_0(\bar x) - \bar x\alpha_0 I_1(\bar x)], \\
e_1(\rho) &= -\mathrm{e}^{-(\bar\gamma+\rho)}[\alpha_0\bar x I_0(\bar x) + (-\alpha_0\rho - \alpha_0\bar\gamma)I_1(\bar x)], \\
e_2(\rho) &= -\mathrm{e}^{-(\bar\gamma+\rho)}[(\tfrac{1}{2}\alpha_0 - \tfrac{1}{4}\alpha_0\bar\gamma - \tfrac{1}{4}\alpha_0\rho)I_0(\bar x) \\
&\quad +\tfrac{3}{8}\alpha_0\bar x I_1(\bar x) + (\tfrac{1}{2}\alpha_0 - \tfrac{1}{4}\alpha_0\bar\gamma - \tfrac{1}{4}\alpha_0\rho)I_2(\bar x) + \tfrac{1}{8}\alpha_0\bar x I_3(\bar x)], \\
e_3(\rho) &= -\mathrm{e}^{-(\bar\gamma+\rho)}[(\tfrac{1}{2}\alpha_0 - \tfrac{1}{4}\alpha_0\bar\gamma - \tfrac{1}{4}\alpha_0\rho - \tfrac{1}{8}\bar x\alpha_0)I_0(\bar x) \\
&\quad -(\tfrac{1}{2}\alpha_0 - \tfrac{1}{4}\alpha_0\bar\gamma - \tfrac{1}{4}\alpha_0\rho - \tfrac{1}{4}\bar x\alpha_0)I_1(\bar x) - \tfrac{1}{8}\bar x\alpha_0 I_2(\bar x)].
\end{aligned}
$$

## References


Argon, A. S. & Im, J. 1975 Separation of second phase particles in spheroidized 1045 steel, cu-0.6 pct cr alloy, and maraging steel in plastic straining. *Metall. Trans.* A **6**, 839–851.

Argon, A. S., Im, J. & Safoglu, R. 1975 Cavity formation from inclusions in ductile fracture. *Metall. Trans.* A **6**, 825–837.

Ball, J. M. 1982 Discontinuous equilibrium solutions and cavitation in nonlinear elasticity. *Phil. Trans. R. Soc. Lond.* A **306**, 557–611.

Cox, T. B. & Low, J. R. 1974 An investigation of the plastic fracture of AISI 4340 and 18 nickel-200 grade maraging steels. *Metall. Trans.* **5**, 1457–1470.

Ferrante, J., Smith, J. R. & Rose, J. H. 1982 Universal binding energy relations in metallic adhesion. In *Microscopic aspects of adhesion and lubrication* (ed. J. M. Georges), pp. 19–30. New York: Elsevier.

Fisher, J. R. & Gurland, J. 1981 Void nucleation in spheroidized carbon steels. 2. model. *Metal Sci.* **15**, 193–202.

Goods, S. H. & Brown, L. M. 1979 The nucleation of cavities by plastic deformation. Acta. Metall. **27**, 1–15.

Gradshteyn, I. S. & Ryzhik, I. M. 1994 In *Table of integrals, series and products* (ed. A. Jeffrey). New York: Academic.

Griffith, A. A. 1920 The phenomena of rupture and flow in solids. *Phil. Trans. R. Soc. Lond.* A **221**, 163–198.

Guckenheimer, J. & Holmes, P. 1983 *Nonlinear oscillations, dynamical systems, and bifurcations of vector fields*. Berlin: Springer.

Gurtin, M. E. 1984 The linear theory of elasticity. In *Mechanics of solids* (ed. C. Truesdell), vol. 2, pp. 1–273. Berlin: Springer.

Hahn, G. T. & Rosenfield, A. R. 1966 Effects of second-phase particles on ductility. Air Force Materials Laboratory Technical Report AFML-TR-65-409.

Hirsch, M. W. & Smale, S. 1974 *Differential equations, dynamical systems and linear algebra*. New York: Academic.






PHILOSOPHICAL TRANSACTIONS OF THE ROYAL SOCIETY A MATHEMATICAL, PHYSICAL & ENGINEERING SCIENCES

Horgan, C. O. & Polignone, D. A. 1995 Cavitation in nonlinear elastic solids: a review. *Appl. Mech. Rev.* **48**, 471–485.

Knops, R. J. & Wilkes, E. W. 1973 Theory of elastic stability. In *Mechanics of solids* (ed. C. Truesdell), vol. 3, pp. 125–302. Berlin: Springer.

Levy, A. J. 1991 The debonding of elastic inclusions and inhomogeneities. *J. Mech. Phys. Solids* **39**, 477–505.

Levy, A. J. 1993 Corrigendum. *J. Mech. Phys. Solids* **41**, 213.

Levy, A. J. 1994 Separation at a circular interface under biaxial load. *J. Mech. Phys. Solids* **42**, 1087–1104.

Levy, A. J. 1995 Nonsymmetric cavity formation at a circular inclusion under remote equibiaxial load. *J. Mech. Phys. Solids* **43**, 1003–1024.

Levy, A. J. 1996 The effective dilatational response of fiber reinforced composites with nonlinear interface. *J. Appl. Mech.* **63**, 357–364.

MAPLE 1994 Waterloo Maple Software, Waterloo.

Mikhlin, S. G. 1960 *Linear integral equations*. Delhi: Hindustan Publishing.

Muskhelishvili, N. I. 1953 *Some basic problems of the mathematical theory of elasticity*. Groningen: Noordhoff.

Needleman, A. 1987 A continuum model for void nucleation by inclusion debonding. *J. Appl. Mech.* **54**, 525–531.

Nutt, S. R. & Needleman, A. 1987 Void nucleation at fiber ends in Al-SiC composites. *Scripta Met.* **21**, 705–710.

Press, W. H., Teukolsky, S. A., Vetterling, W. T. & Flannery, B. P. 1992 *Numerical recipes in fortran*. Cambridge University Press.

Rogers, H. C. 1960 The tensile fracture of ductile metals. *AIME Trans.* **218**, 498–506.

Tanaka, K., Mori, T. & Nakamura, T. 1970 Cavity formation at the interface of a spherical inclusion in a plastically deformed matrix. *Phil. Mag.* **21**, 267–279.

Tricomi, F. G. 1985 *Integral equations*. New York: Dover.

Watson, G. N. 1995 *A treatise on the theory of Bessel functions*. Cambridge University Press.

Wiggins, S. 1990 *Introduction to applied nonlinear dynamical systems and chaos*. Berlin Springer.

*Received 16 January 1996; accepted 10 October 1996*





PHILOSOPHICAL TRANSACTIONS OF THE ROYAL SOCIETY A MATHEMATICAL, PHYSICAL & ENGINEERING SCIENCES